THE ASTRONOMICAL JOURNAL, 120:1499–1515, 2000 September

DETAILED ANALYSIS OF EARLY TO LATE-TIME SPECTRA OF SUPERNOVA 1993J

THOMAS MATHESON,[1] ALEXEI V. FILIPPENKO,[1] LUIS C. HO,[2] AARON J. BARTH,[3] AND DOUGLAS C. LEONARD[1]

Received 2000 March 5; accepted 2000 June 8

ABSTRACT

We present a detailed study of line structure in early to late-time spectra of supernova (SN) 1993J. Spectra during the nebular phase, but within the first two years after explosion, exhibit small-scale structure in the emission lines of some species, notably oxygen and magnesium, showing that the ejecta of SN 1993J are clumpy. On the other hand, a lack of structure in emission lines of calcium implies that the source of calcium emission is uniformly distributed throughout the ejecta. These results are interpreted as evidence that oxygen emission originates in clumpy, newly synthesized material, while calcium emission arises from material preexisting in the atmosphere of the progenitor. Spectra spanning the range 433–2454 days after the explosion show boxlike profiles for the emission lines, clearly indicating circumstellar interaction in a roughly spherical shell. This is interpreted within the Chevalier & Fransson model for SNe interacting with mass lost during prior stellar winds. At very late times, the emission lines have a two-horned profile, implying the formation of a somewhat flattened or disklike structure that is a significant source of emission. The very high signal-to-noise ratio spectra are used to demonstrate the potential significance of misinterpretation of telluric absorption lines in the spectra of bright SNe.

Key words: circumstellar matter — stars: mass loss — supernovae: general — supernovae: individual (SN 1993J) — techniques: spectroscopic

1. INTRODUCTION

Supernova 1993J presented a great opportunity in the study of supernovae (SNe). It occurred in the nearby galaxy M81 (NGC 3031; $d = 3.6$ Mpc; Freedman et al. 1994) and reached a maximum brightness of $m_V = 10.8$ mag (e.g., Richmond et al. 1996). This allowed extremely detailed observations to be taken over a long time interval. The fact that SN 1993J underwent a transformation from a Type II to a Type IIb, strengthening the link between SNe II and SNe Ib as core-collapse events, only enhanced the importance of this object (see, e.g., Wheeler & Filippenko 1996; Matheson et al. 2000, hereinafter Paper I, for detailed discussions of the nature of SN 1993J).

We have previously presented analyses of the spectra of SN 1993J obtained during its first year (Filippenko, Matheson, & Ho 1993, hereinafter FMH93; Filippenko, Matheson, & Barth 1994, hereinafter FMB94), while Paper I shows our complete low-resolution spectroscopic data set. The early spectra and the transition from SN II to SN IIb are covered by FMH93, while the onset of the nebular phase and the beginning of signs of circumstellar interaction are discussed by FMB94. In this paper, we take a closer look at the details of some of the earlier spectra and we present the analysis of late-time spectra of SN 1993J. The clumpy nature of SN 1993J, as revealed in the details of spectra from early to nebular times, is presented in § 2. The late-time spectra and their evidence of circumstellar interaction are discussed in § 3; we summarize our conclusions in § 4. In the Appendix, we discuss the potential impact of telluric absorption on the interpretation of the spectra of bright SNe and the implications this has for future SN studies.

All of the low-dispersion spectra discussed herein were obtained at the Lick and Keck observatories. In addition, a single high-dispersion spectrum was obtained using the Keck I 10 m telescope. The details of the observations, including instrumental configuration, dates of observation, and observational parameters, are presented in Paper I. We follow Lewis et al. (1994) in adopting 1993 March 27.5 UT (JD 2,449,074) as the date of explosion.

2. CLUMPS

2.1. *Clumps in Other Supernovae*

The mottled appearance of supernova remnants (SNRs) has often been interpreted as evidence for clumps in the ejecta of SNe. For example, fast-moving features have been identified in Cas A for quite some time (e.g., Baade & Minkowski 1954), and modern studies continue to interpret the structure of Cas A as the result of clumpy SN ejecta (e.g., Anderson et al. 1994). The discovery of metal-enriched fragments outside the boundary of the Vela SNR (Aschenbach, Egger, & Trümper 1995), a high-velocity "bullet" in Vela (Strom et al. 1995), and fast-moving oxygen filaments in Puppis A (and other remnants; Winkler & Kirshner 1985 and references therein) all support the contention that SN ejecta are clumped. There is also a theoretical underpinning for the expectation of clumps in the ejecta of core-collapse SNe. This includes the necessity of mixing in SNe Ib/c (e.g., Wheeler et al. 1987; Shigeyama et al. 1990; Hachisu et al. 1991) and the presence of instabilities, such as convective instabilities in neutrino-driven explosion mechanisms and Rayleigh-Taylor instabilities during the expansion of the ejecta (e.g., Kifonidis et al. 2000 and references therein). In fact, with a small core mass (3–4 $M_\odot$), SN 1993J should have relatively large Rayleigh-Taylor instabilities that mix the core (Iwamoto et al. 1997).

The observation of small-scale structure in SN line emission requires a spectrum with a high signal-to-noise ratio

[1] Department of Astronomy, University of California at Berkeley, Berkeley, CA 94720-3411; matheson@astron.berkeley.edu, alex@astron.berkeley.edu, leonard@astron.berkeley.edu.

[2] The Observatories of the Carnegie Institution of Washington, 813 Santa Barbara Street, Pasadena, CA 91101-1292; lho@ociw.edu.

[3] Harvard-Smithsonian Center for Astrophysics, 60 Garden Street, Cambridge, MA 02138; abarth@cfa.harvard.edu.

(S/N) and the spectral resolution to distinguish narrow features. This in turn necessitates a bright source and an efficient detector with at least moderate dispersion ($\sim$1–10 Å pixel^{-1}). These two requirements for SNe were first fulfilled with SN 1985F. Analysis of spectra of the Type Ib SN 1985F revealed several distinct clumps in the [O I] $\lambda\lambda$6300, 6364 lines as well (Filippenko & Sargent 1989). These clumps had widths $\sim$100–250 km s^{-1} with amplitudes of 2%–10%. The small-scale features changed slightly over time, becoming narrower and relatively stronger. The Mg I] λ4571 also had features, but they did not match those of the oxygen lines.

The bright, nearby SN 1987A provided another opportunity to study SN spectra in detail. While examining the [O I] $\lambda\lambda$6300, 6364 doublet of SN 1987A, Stathakis et al. (1991) discovered what appeared to be a sawtooth profile on the tops of the lines: there were $\sim$50 small-scale features with a typical size of 80 km s^{-1} (FWHM) and amplitudes of 3%–10% of the global line profile. The structures persisted over time and were consistent between the two doublet lines. Clumps were also observed in the Hα line (Hanuschik et al. 1993). These had widths of 400–500 km s^{-1} with amplitudes of 7%–10% of the overall line strength. The Hα clumps were present over several hundred days, but individual clumps were not persistent. Hanuschik et al. (1993) interpreted this as changes in the level of dust extinction along the lines of sight to the individual clumps. Spyromilio & Pinto (1991) found that the oxygen density derived from the line intensity ratios of [O I] λ6300 and [O I] λ6364 gave too large an oxygen mass if the oxygen filled the entire volume suggested by the expansion velocity; a low filling factor for oxygen was consistent with the calculated density, volume at that epoch, and a reasonable oxygen mass. Such a low filling factor can be interpreted as clumpiness. Further evidence for clumps in the ejecta of SN 1987A is presented by Spyromilio, Stathakis, & Meurer (1993), who found a common feature in emission lines of Hα, [Fe II] λ7155, and [Ca II] $\lambda\lambda$7291, 7324. Clumps were also seen at later times in infrared (IR) emission lines of iron in SN 1987A (Spyromilio, Meikle, & Allen 1990; Haas et al. 1990). The pattern seen in the oxygen lines was not replicated in these other species.

The Type II SN 1988A may also have had clumps. They were not apparent in the spectra, but following the analysis of the [O I] $\lambda\lambda$6300, 6364 doublet in SN 1987A of Spyromilio & Pinto (1991), Spyromilio (1991) derived a low filling factor for oxygen in SN 1988A of 0.05, and thus deduced a clumpy nature for the source of the oxygen emission. In addition, Fassia et al. (1998) invoked clumps of helium to explain the strength of He I λ10830 line in the Type II SN 1995V given their model of ^{56}Ni mixing, although the clumps were not evident from the spectra.

SN 1993J, as noted before, was extremely bright, so any clumps in its spectrum should be readily detectable. Li et al. (1994) reported clumps in their spectra of SN 1993J. Wang & Hu (1994) noted the presence of narrow components in the forbidden lines of oxygen, and they used the clumpy nature of the SN to explain apparent blueshifts in the emission lines of [O I] λ5577 and [O I] λ6300. Spyromilio (1994, hereinafter S94) presented a much more detailed analysis of the clumps visible in the spectra of SN 1993J and also concluded that there is large-scale anisotropy in the SN based on the blueshifts of the lines (oxygen and magnesium) as well as the differences in the distribution of clumps both between and within the observed atomic species. This interpretation of the blueshifts was questioned by Houck & Fransson (1995), however. They concluded that the blueshifts are only apparent, and did not represent physical asymmetries in the lines. The [O I] $\lambda\lambda$6300, 6364 doublet can be dramatically affected by scattering of Hα if oxygen and hydrogen are distributed in shells, and this would mimic the observed asymmetry. Blending affects the other lines, with [O I] λ5577 contaminated by [Fe II] λ5536 and [Co II] λ5526. The Mg I] λ4571 line is affected by Fe II multiplets near 4600 Å.

2.2. *Analysis of the Clumps*

As the brightest supernova in the northern hemisphere since SN 1954A, SN 1993J provided an object for which high S/N spectra could be obtained over an extended period of time. Any intrinsic small-scale structure in the emission lines of SNe is normally lost in the noise of the spectra. For SN 1993J, the noise over most of our range (3500–9000 Å) does not obscure the small-scale features in the spectra until several hundred days after the explosion. This allows us to make an extensive study of line substructure as the supernova evolves. Telluric absorption could introduce spurious small-scale structure, but we attempt to remove its effects (see Appendix).

Careful inspection of the spectra of SN 1993J reveals small-scale structure in many emission lines, especially [O I] $\lambda\lambda$6300, 6364, [O I] λ5577, O I λ7774, Mg I] λ4571, and [Ca II] $\lambda\lambda$7291, 7324. The [O I] $\lambda\lambda$6300, 6364 lines in particular show a distinctive sawtooth profile similar to those described above for SN 1987A and SN 1985F (Fig. 1). Note that all spectra have had the systemic velocity of SN 1993J removed ($-$140 km s^{-1}, determined from narrow lines in early-time spectra; see, e.g., FMH93). To isolate these fluctuations, we removed the global shape of the underlying line by smoothing the profile, and then subtracting the smoothed version. The spectra were smoothed with a running boxcar with a width of 60 Å—wide enough to remove the small-scale fluctuations from the line profile, but narrower than the line itself, so that the subtraction would leave only the small features. This is the same method employed by Filippenko & Sargent (1989) to isolate similar substructure in the [O I] $\lambda\lambda$6300, 6364 lines of SN 1985F, although they used a smaller boxcar width for smoothing

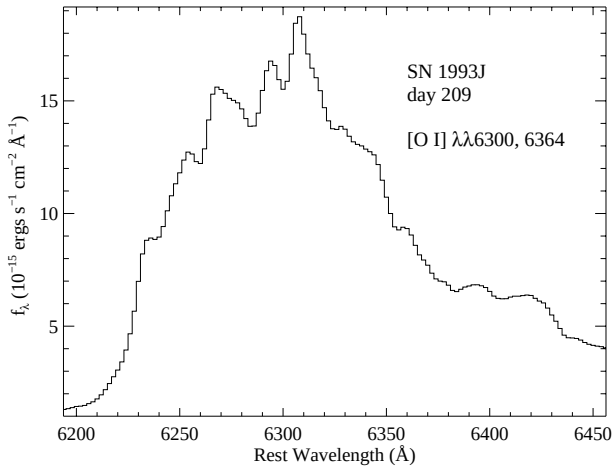

FIG. 1.—Spectrum of the [O I] $\lambda\lambda$6300, 6364 blend on day 209. Note the sawtooth structure superposed on the global line profile.

that was better matched to the velocity width of the fluctuations in SN 1985F.

Such a technique is similar to the process of unsharp masking in Fourier space. We experimented with this and other methods in the Fourier domain to isolate high-frequency components of spectra. The results were not superior to the smoothing technique. Moreover, the Fourier techniques became less successful as the relative noise level increased in later spectra. The subtraction of a smoothed line from itself does, however, introduce an artifact in the resulting residuals due to poor removal of the edges of the global line profile. These artifacts have a different character than the legitimate fluctuations; they are broader and generally show a gradual decrease from the subtracted continuum. Once an actual feature is reached, it clearly stands out from the edge effect. This is illustrated in Figure 2 with an artificial profile from which the smoothing technique isolates the six introduced components. The edge effects are prominent, but distinctly different in velocity width and character from the actual fluctuations. To eliminate the edge effects would require a model of the underlying line profile. This model would vary from line to line, and would also change over time as different amounts of nearby lines contaminate the feature under consideration. For example, as illustrated in Figure 4 of FMB94, the relative levels of [O I] $\lambda\lambda$6300, 6364 and Hα λ6563 can change dramatically over a time scale of months. Subtracting a different line profile for different spectra at different times could introduce spurious components or temporal differences. In the interest of consistency, we chose to use the smoothing technique to identify substructure in the lines. In no case did it fail to find components visible in the original spectra, and the only new features introduced are the edge effects that are easily distinguishable from genuine components.

Figure 3 shows a typical example of the clumps in the [O I] $\lambda\lambda$6300, 6364 lines on day 209. There are five distinctive maxima marked in the figure. S94 found six clumps, but his clump *f* (at $\sim$2900 km s^{-1}) is difficult to discern in this doublet; his clumps *a*, *b*, *c*, *d*, and *e* correspond to our clumps 5, 4, 3, 2, and 1. For the [O I] λ6300 line, these clumps are at velocities of (starting from the blueshifted edge) -3220, -2340, -1510, -310, and 410 km s^{-1} (where 6300 Å defines zero velocity). The marked minima (identified as 6, 7, and 8) have velocities of -2750, -1930, and -740 km s^{-1}, respectively. The uncertainty in the values for the velocities of clumps is $\sim$50 km s^{-1}. The corresponding locations of these components for the [O I] λ6364 line are also indicated, but the features themselves are difficult to distinguish. There is also an emission feature at $\sim$2000 km s^{-1}, but it is unclear if this is from [O I] λ6300, [O I] λ6364, both, or Hα. In fact, the large velocity width of Hα at these times (FWHM $\approx$ 17,000 km s^{-1}, full width at zero intensity [FWZI] $\approx$ 23,000 km s^{-1}, FMB94; see also below) significantly contaminates the spectrum to a blue wavelength of at least 6375 Å, possibly as far as 6310 Å. The presence of Hα throughout the region of the spectrum where one would find [O I] λ6364 makes the identification of the [O I] λ6364 clumps problematic at best.

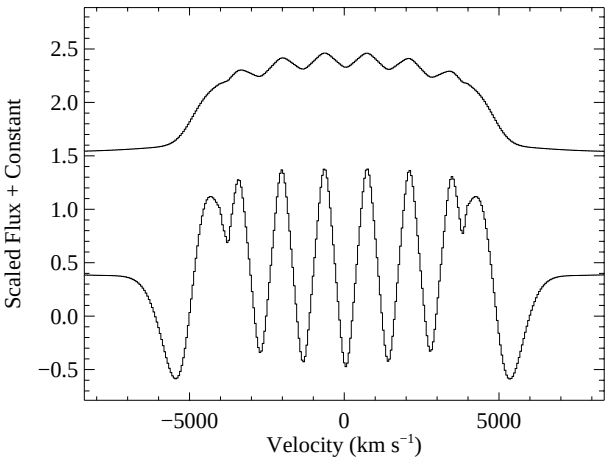

FIG. 2.—Artificial spectral line with six clumps added. The lower spectrum indicates the result of the smoothing and subtraction technique described in the text. The six clumps are readily apparent, along with the edges of the line, although the edges look distinctly different from the clumps. For this, and all subsequent figures of smoothed and subtracted line profiles, the flux-density scaling is linear but arbitrary; the profiles are offset by arbitrary, additive amounts.

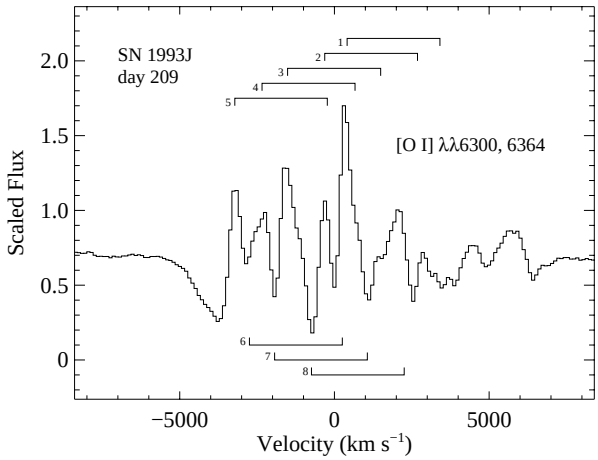

FIG. 3.—Smoothed and subtracted [O I] $\lambda\lambda$6300, 6364 line on day 209. Pairs of maxima and minima with the same relative velocity for the [O I] λ6300 and [O I] λ6364 lines are indicated. The zero point for velocity is 6300 Å. See discussion in the text.

The [O I] $\lambda\lambda$6300, 6364 clumps described above first become obvious in our day 93 spectrum. They are not apparent on day 45. As can be seen in Figure 4, once the features appeared, they remain consistent until day 433. Beyond that day, the clumps may still be present, but the supernova had faded to the point that it was difficult to obtain spectra with a S/N high enough to distinguish the clumps. The clumps at -2340 and 410 km s^{-1} are, in fact, not obvious even in the day 433 spectrum. There are some slight changes in the individual clumps. The clump at -1510 km s^{-1} appears to broaden slightly, from 370 km s^{-1} on day 93 (all widths are FWHM) to 470 km s^{-1} on day 167, while increasing in amplitude in comparison with the other clumps. The amplitude increase continues past day 167 to the time when it became difficult to distinguish the clumps. The clump at -310 km s^{-1} grows considerably in relative strength, by almost a factor of two from day 93 to day 433. The clump at 410 km s^{-1} narrows from 540 km s^{-1} on day 93 to 390 km s^{-1} on day 167, after which it remains constant.

The features seen in the [O I] $\lambda\lambda$6300, 6364 lines are also found in other oxygen emission lines. Figure 5 compares [O I] $\lambda\lambda$6300, 6364 with [O I] λ5577 and O I λ7774. The clumps line up quite well between [O I] λ6300 and [O I]

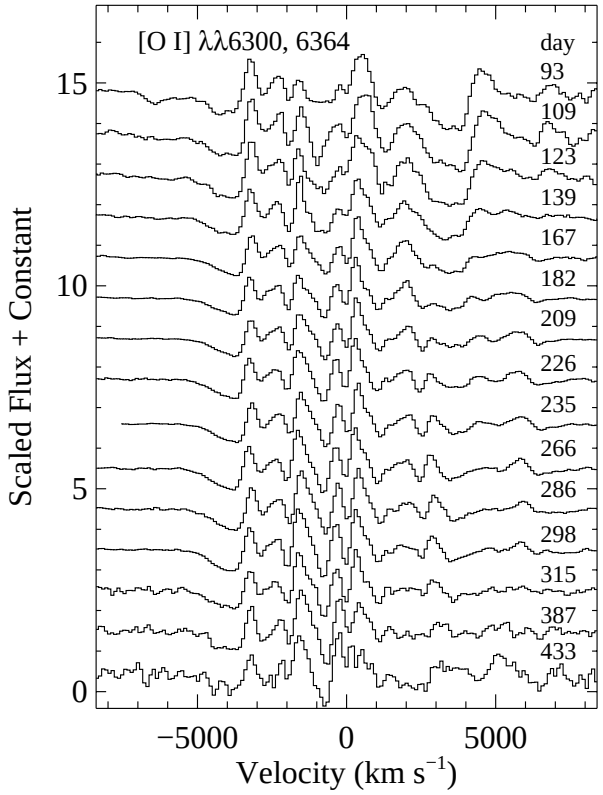

FIG. 4.—Time evolution of the [O I] λλ6300, 6364 line from day 93 to day 433. The zero point for velocity is 6300 Å. Note the remarkable consistency of the substructure in the line.

λ5577. Li et al. (1994) found a similar correspondence for a single epoch. The only significant differences are slight changes in relative intensity of some of the clumps (compare the clumps at −310 and 410 km s^{-1} in [O I] λ6300 and [O I] λ5577). These may suggest intrinsic differences in physical conditions in the two clumps, but are more likely the result of contamination of the lines by other species (see above and Houck & Fransson 1996 for a discussion of potential line contaminants in SN 1993J). S94's clump *f* at ∼2900 km s^{-1} is apparent in [O I] λ5577 and O I λ7774. The O I λ7774 line is missing the −2340 km s^{-1} component completely, and the −3220 km s^{-1} clump is actually at −3110 km s^{-1}, slightly redshifted in comparison with the other oxygen lines. The shift of a clump is most likely the result of contamination, but the absence of one clump from O I λ7774 that is clearly evident in [O I] λ6300 and [O I] λ5577 is puzzling. The O I λ7774 line is contaminated by telluric absorption (see Appendix), but this is not likely to result in the apparent loss of a single component, especially not consistently over many epochs. The difficulty in determining actual flux values for the clumps effectively precludes any evaluation of the differing physical parameters for the various clumps, but the changing physical conditions from clump to clump are most likely the cause of the slight differences seen when comparing the various oxygen lines. In addition, the contamination of all the lines makes even global evaluations highly uncertain.

There is evidence for clumps in lines of other species. Figure 6 shows the small-scale structure of Mg I] λ4571 from day 139 to day 298, while Figure 7 shows them for [Ca II] λλ7291, 7324 from day 123 to day 298 (7291 Å defines the zero velocity for calcium). (The fact that small-scale fluctuations in magnesium and calcium lines are visible for only a subset of the number of days that they are present in oxygen is more indicative of the vagaries of observation than a difference in the physical conditions producing the lines; earlier spectra are contaminated by other lines, while later spectra are noisier.) Again, the features are fairly consistent over time, but, as Figure 8 shows

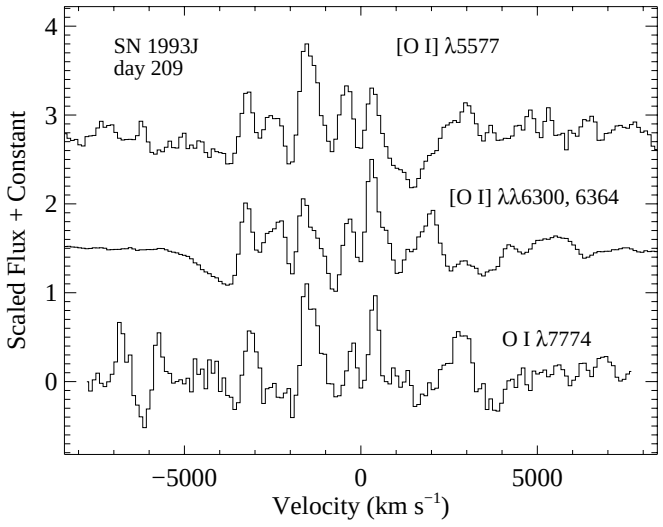

FIG. 5.—Comparison of the clumps in the [O I] λ5577, [O I] λλ6300, 6364, and O I λ7774 emission lines on day 209. The zero point for velocity for [O I] λλ6300, 6364 is 6300 Å. All three have the same basic structure, although the one permitted line (λ7774) is missing the component at −2340 km s^{-1}; see text for details.

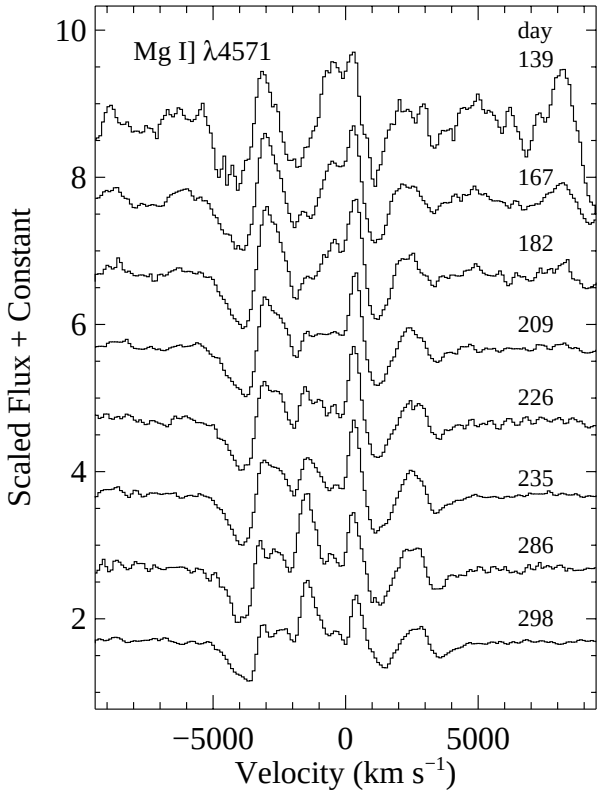

FIG. 6.—Time evolution of the Mg I] λ4571 line from day 139 to day 298. The major clumps persist over time, but there are changes in the details of the substructure.

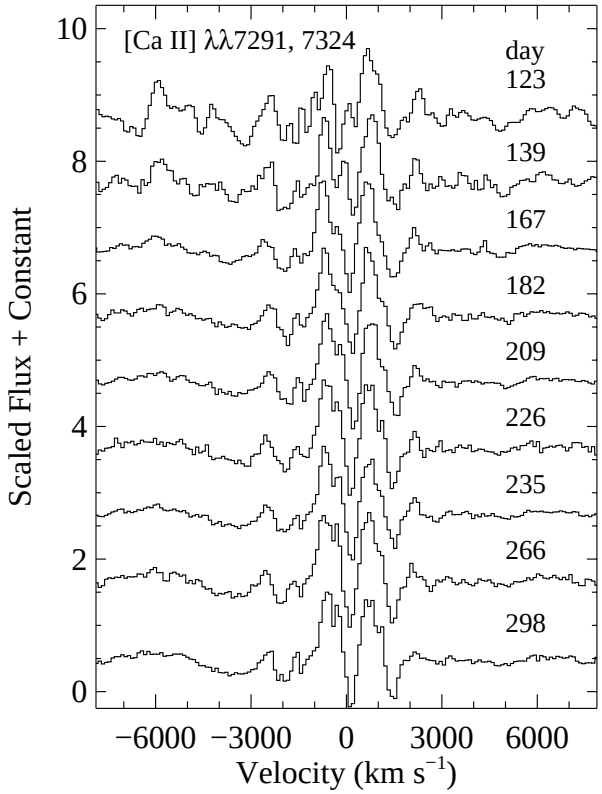

FIG. 7.—Time evolution of the [Ca II] λλ7291, 7324 line from day 123 to day 298. The zero point for velocity is 7291 Å. The two components of the doublet stand out over the entire series, with relatively little other structure.

in a detailed comparison of [O I] λλ6300, 6364, Mg I] λ4571, [Ca II] λλ7291, 7324, and Hα on day 209, the pattern in the clumps is very different between the species, although Li et al. (1994) found that some features did correspond between Hα and [O I] λ6300. Figure 9 shows [O I] λλ6300, 6364, Hα, and Mg I] λ4571 from day 433, and the differences between the lines are even more apparent. The Hα line will

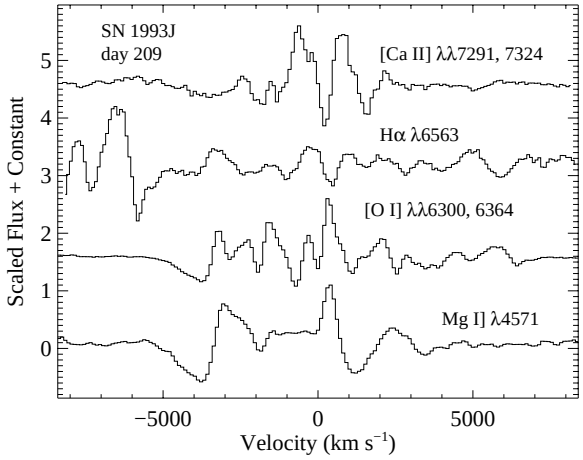

FIG. 8.—Comparison of the clumps in [Ca II] λλ7291, 7324, Hα, [O I] λλ6300, 6364, and Mg I] λ4571 on day 209. The zero point for velocity for [O I] λλ6300, 6364 is 6300 Å, while that for [Ca II] λλ7291, 7324 is 7291 Å. The individual clumps in each species do not appear correlated. The magnesium line may show some clumps that line up with oxygen. Calcium and hydrogen are distinctly different.

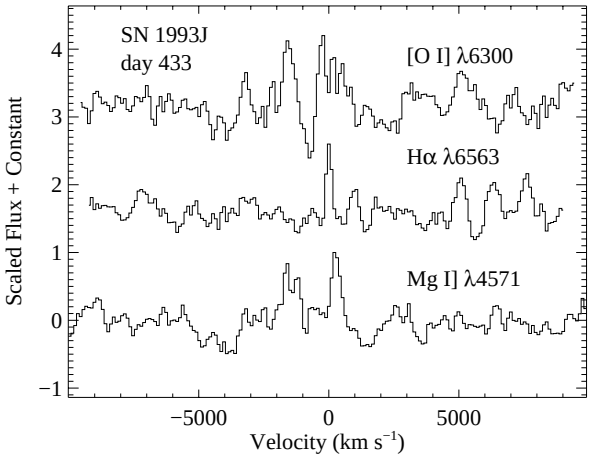

FIG. 9.—Comparison of the clumps in [O I] λλ6300, 6364, Hα, and [Mg I] λ4571 on day 433. The zero point for velocity for [O I] λλ6300, 6364 is 6300 Å. By late times, there is no correspondence between the lines for the substructure. Note the narrow component of Hα at zero velocity.

be discussed in more detail in § 3. The Mg I] λ4571 line does have one clump (410 km s^{-1}) that lines up with oxygen, but the rest of the structure is very different, with relatively fewer fluctuations, as in SN 1985F (Filippenko & Sargent 1989). (The minimum at −2740 km s^{-1} in [O I] λλ6300, 6364 marginally lines up with a minimum in Mg I] λ4571, but it is probably coincidental.) This may indicate that the magnesium and oxygen emission arise from substantially different clumps.

The [Ca II] λλ7291, 7324 lines have some substructure, but they are relatively smooth. Aside from the peaks of the two lines and the edge effects described above, there is very little small-scale structure that is consistent. There is a small peak at about −1700 km s^{-1}, but no other significant evidence for persistent clumps. In addition, these lines coincide with a telluric water absorption feature (see Fig. 16), so incomplete removal of the water band profile may contaminate this region.

The scale of the clumps is not hidden by the resolution of the observations. The low-dispersion spectra used here have typical resolutions of 6–7 Å (FWHM). At 6300 Å, that corresponds to ∼300 km s^{-1}. Comparison with the high-resolution HIRES spectrum illustrates that there is little, if any, substructure with scales smaller than this (see Fig. 9 of Paper I). Virtually all the clumps that are apparent in the HIRES spectrum appear in the low-dispersion spectrum taken four days later. The clumps that appear with lower contrast in the low-dispersion spectrum, but are easily found using our smoothing technique, do stand out more clearly in the HIRES spectrum. The HIRES spectrum shows that we are not missing any of the significant details of the clumps in the low-resolution spectra.

2.3. *Discussion of the Clumps*

The contrast between the presence of clumps in the emission lines of oxygen (and other species) and the relative smoothness of the calcium emission lines implies that the sources of emission for the various species are distributed differently in the supernova ejecta. One possibility is that the oxygen emission arises in distinct clumps of material while the source of calcium emission is distributed uniformly throughout the ejecta. While attempting to model

the [O I] $\lambda\lambda$6300, 6364 lines and the Ca II lines ([Ca II] $\lambda\lambda$7291, 7324 and the near-IR triplet), Li & McCray (1992, 1993) developed a similar concept to explain the structure seen in emission lines of SN 1987A that parallel those described above for SN 1993J.

Li & McCray (1992) initially focused on the forbidden oxygen lines. They developed a model based upon the relative line strengths at a given epoch for the [O I] $\lambda\lambda$6300, 6364 doublet that predicted a value for the total oxygen mass to filling-factor ratio. By choosing a reasonable value for the total oxygen mass (from theoretical models), they concluded that the oxygen emission must come from clumps distributed uniformly throughout the ejecta with a small filling factor. The clumps would develop from material synthesized in earlier evolution or during the explosion itself. As already mentioned, fast-moving oxygen components are seen in SNRs (Winkler & Kirshner 1985). When Li & McCray (1993) subsequently analyzed the calcium lines, they found that the observed lines were too weak given the probable amount of calcium produced during prior evolution and from explosive nucleosynthesis. Li & McCray hypothesized that clumps of calcium do form but do not contribute to the emission. These clumps of calcium intercept γ-ray radiation in proportion to their mass fraction. As this fraction is small, they receive only a small amount of radioactive luminosity and thus they do not achieve temperatures necessary for emission, although oxygen lines can be excited at these temperatures. The preexisting envelope of the star is heated generally as hydrogen and helium do not radiate efficiently, allowing calcium that was thoroughly mixed into the atmosphere, most likely present from the time of the progenitor's formation, to reach the temperatures required to produce Ca II emission.

This scenario of emission from smoothly distributed, preexisting calcium while oxygen is clumped with a small filling factor explains the detailed line structure seen in SN 1993J. Other attempts to model the spectra of SN 1987A, however, concluded that the source of the oxygen emission consisted chiefly of the envelope, and so was also the result of preexisting constituents (Swartz, Harkness, & Wheeler 1989; Swartz 1991), although later analysis by the same authors acknowledged that some oxygen from the core may contribute to the emission and that it might be clumped (Wheeler, Swartz, & Harkness 1993). Smoothly distributed oxygen is difficult to reconcile with the clumps exhibited by the oxygen-line profiles. The underlying smooth line may be the result of the preexisting oxygen, but clumps are clearly present in SN 1993J and SN 1987A, implying that there is a distinct difference in the site of oxygen and calcium emission.

The sawtooth appearance of the [O I] $\lambda\lambda$6300, 6364 lines indicates a rough scale for the size of the clumps in the ejecta. Chugai (1994) used similar data for SN 1987A to develop a technique for determining the oxygen mass. Given the minimum cloud size (on a velocity scale), the total velocity width of the lines, and the relative level of fluctuation in the clumps (the scale of the clumps compared to the overall line strength), one can then estimate the filling factor of the clumps ($f \approx 0.1$ in the case of SN 1987A). Several groups used the relative ratio of the [O I] $\lambda\lambda$6300, 6364 lines in SN 1987A to derive an oxygen mass to filling-factor ratio (M_O/f) of 11 $M_\odot$ (Li & McCray 1992) to 15 $M_\odot$ (Spyromilio & Pinto 1991; Chugai 1992; Andronova 1992). This implies a total oxygen mass of 1.1–1.5 $M_\odot$ (Chugai 1994). As the line widths for SN 1993J are much larger (FWHM $\approx$ 5400 km s^{-1} for SN 1993J on day 167 vs. FWHM $\approx$ 2700 km s^{-1} for SN 1987A on day 173; Li & McCray 1992), the two doublet lines are blended, as well as severely affected by the broad Hα line, and this effectively precludes a new evaluation for M_O/f. If one makes the admittedly dangerous assumption that this ratio is relatively constant among core-collapse SNe, then Chugai's method can be applied. For SN 1993J, the sizes of the clumps imply a typical cloud radius (in velocity space) of 150 km s^{-1} with a relative fluctuation compared to the total line flux of $\delta F/F \approx 0.1$. To estimate the effective radius (in velocity space) for Chugai's calculation, we use Li & McCray's (1992) definition that emission at $|v| \lesssim v_{\rm eff}$ constitutes 90% of the flux in the line (Li & McCray refer to $v_{\rm eff}$ as the "expansion velocity"). For SN 1993J, the FWHM is $\sim$5400 km s^{-1}, and, assuming a Gaussian profile for the line, this implies that 90% of the emission of the line comes from within $v \approx \pm 3800$ km s^{-1}. With $v_{\rm eff} \approx 3800$ km s^{-1}, we find a filling factor of 0.06 by Chugai's method. Using the oxygen mass to filling-factor ratios derived for SN 1987A, these clump parameters yield an oxygen mass of 0.7–0.9 $M_\odot$ for SN 1993J.

The preferred models of Nomoto et al. (1993) and Shigeyama et al. (1990) for SN 1993J predict an oxygen mass of $\sim$0.4 $M_\odot$. This is similar to the value of 0.47 $M_\odot$ for oxygen in the model of Swartz et al. (1993). The models of Woosley et al. (1994) and Woosley, Langer, & Weaver (1995) yield 0.5–0.7 $M_\odot$ for SN 1993J. Utrobin (1994) finds a smaller value for the oxygen mass of $\sim$0.2 $M_\odot$, but also predicts a slightly narrower velocity profile for the oxygen lines ($v \lesssim$ 4600 km s^{-1}); the day 167 spectrum has a blue edge for the [O I] λ6300 line that indicates an expansion velocity of $\sim$4900 km s^{-1}. For SN 1987K, another Type IIb SN, Schlegel & Kirshner (1989) found an oxygen mass of $\sim$0.3 $M_\odot$. The value we derive for SN 1993J is probably a bit high, but the blanket assumption that M_O/f is constant among core-collapse SNe definitely increases the uncertainty of the result. A slightly smaller M_O/f ratio would make our derived oxygen mass entirely consistent with the model predictions.

3. LATE-TIME SPECTRA

3.1. *Late-Time Studies of Supernovae*

Few SNe have had relatively frequent spectroscopic observations for more than three years. Several have have been recovered many years (even decades) after explosion. These include SN 1957D (Long, Blair, & Krzeminski 1989; Cappellaro, Danziger, & Turatto 1995), SN 1970G (Fesen 1993), SN 1978K (Ryder et al. 1993; Chugai, Danziger, & Della Valle 1995; Chu et al. 1999), SN 1979C (Fesen & Matonick 1993; Fesen et al. 1999, hereinafter F99), SN 1980K (Fesen & Becker 1990; Leibundgut et al. 1991; Uomoto 1991; Fesen & Matonick 1994; F99), SN 1985L (Fesen 1998), SN 1986E (Cappellaro et al. 1995), SN 1986J (Leibundgut et al. 1991; Uomoto 1991), and SN 1994aj (Benetti et al. 1998). SN 1988Z showed evidence for circumstellar interaction from its early-time spectra, and continues to be observed spectroscopically with $\sim$10 yr of coverage (Filippenko 1991a, 1991b; Stathakis & Sadler 1991; Turatto et al. 1993; Aretxaga et al. 1999). SN 1987A represents a special case; its proximity allows continued monitoring that would most likely not be possible for this SN if it

were in a more distant galaxy, and so we will exclude it from this discussion[4].

SNe such as SN 1988Z that show the spectroscopic characteristics of circumstellar interaction from an early time do so through very strong, narrow emission, especially in the Balmer lines. They are often referred to as a subclass of SNe II, either as "Seyfert 1" types or the more commonly used Type IIn (Filippenko 1989, 1991a; Schlegel 1990). If we ignore the SNe IIn, and consider only the SNe II observed at very late times that appeared normal initially, then all of the SNe recovered after many years have fairly similar spectra. The precondition of normalcy at maximum brightness is not necessarily applicable to all the SNe listed above, as some (SN 1957D, SN 1978K, and SN 1986J) were not actually observed until much later in their evolution. All but SN 1978K have fairly broad emission lines (FWZI $\approx$ 10,000 km s^{-1}) of Hα, [O III] $\lambda\lambda$4959, 5007, and [O I] $\lambda\lambda$6300, 6364 at late times. Most of these lines show a largely boxlike profile, as expected from an expanding, roughly spherical, shell.

3.2. *Prior Analysis of our Nebular to Late-Time Spectra*

Spectra of SN 1993J up to day 433 are discussed by FMB94. They concluded that evidence for circumstellar interaction is visible as early as day 235 when the boxlike profile of Hα became distinct. This shape is predicted by the circumstellar interaction models of Chevalier & Fransson (1994, hereinafter CF94). Indeed, FMB94 found an Hα luminosity of 4.4×10^{38} ergs s^{-1} on day 433, in approximate agreement with the models of CF94 (and assuming the X-ray luminosity and density profile as described in Fransson, Lundqvist, & Chevalier 1996). There is a considerable amount of evidence for circumstellar interaction in SN 1993J from observations at radio and X-ray wavelengths (see Fransson et al. 1996 and references therein). Houck & Fransson (1996) and Patat, Chugai, & Mazzali (1995) also conclude that circumstellar interaction is present based on late-time optical spectra. The spectra described here are dominated by the effects of circumstellar interaction, and thus are discussed within that context. These late-time spectra are shown in their entirety in Figures 7 and 10 of Paper I.

For our present purposes, we restrict our definition of late-time spectra to those obtained from day 433 onward. Nebular features begin to appear by day 93 (see Figs. 3, 5, and 7 of Paper I), and were noted earlier ($\sim$day 62) by others with better temporal coverage during this period (Barbon et al. 1995). From day 209, the nebular features completely dominate the spectra, although an unusual box-shaped Hα line may also be apparent at that point. This box-shaped line is clearly visible by day 355. From that day, the emission characteristics of the SN begin to be dominated by evidence for circumstellar interaction. Nebular features in the ejecta continue to play a significant role in the spectra, but are less important from day 473 onward. This section will focus on the late-time spectra during this interaction phase, from day 473 to day 2454. Figure 10 displays three high-quality Keck spectra of SN 1993J from days 976, 1766, and 2454 to illustrate the discussion of the late-time spectra.

[4] As of early 2000, though, signs of more circumstellar interaction in SN 1987A are beginning to appear (e.g., Bouchet et al. 2000).

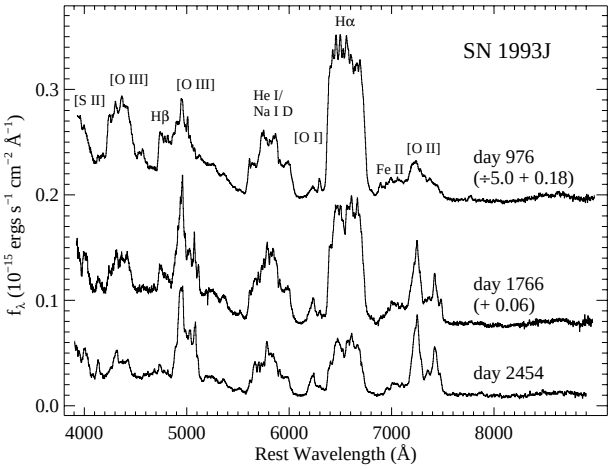

FIG. 10.—Three examples of the late-time spectra of SN 1993J on days 976, 1766, and 2454. The day 976 spectrum was obtained under nonphotometric conditions, and so has been arbitrarily scaled to match the other two. A constant has also been added to the day 976 and day 1766 spectra to offset the spectra from each other. The day 2454 spectrum suffers from minor second-order contamination beyond $\sim$7600 Å. Note the relative increase over time of the oxygen lines in comparison with Hα. In addition, the substructure of the Hα line varies over time, although a small feature at zero velocity persists.

3.3. *Extinction*

Analysis of the late-time spectra depends upon the amount of reddening that affects them. As absolute values for the line fluxes are difficult to obtain, line intensity ratios must suffice, and here the effects of reddening can be extreme. Various values for the extinction were found in photometric and spectroscopic studies of SN 1993J. Wheeler et al. (1993) used reddened blackbody models in comparison with early-time spectra to conclude that $A_V = 0.47 \pm 0.06$ mag [all reported values of A_V assume $R = A_V/E(B-V) = 3.1$]. With similar techniques, Lewis et al. (1994) calculated $A_V = 0.58 \pm 0.05$ mag, while Clocchiatti et al. (1995) found $A_V \approx 0.7$ mag. Richmond et al. (1994) summarized several measurements of the extinction toward M81 in general and SN 1993J in particular. The average value is $A_V \approx 0.6$ mag, but ranges from $A_V = 0.2$ mag to $A_V = 1.0$ mag. Barbon et al. (1995) estimated $A_V = 0.9$ from Na I D line equivalent widths. The Schlegel, Finkbeiner, & Davis (1998) dust maps show that the Galactic component is $A_V = 0.25$ mag, not an insignificant fraction. For the purposes of this discussion, we will take the extinction toward SN 1993J to be $A_V = 0.6$ mag. All fluxes and line ratios will be reported for the spectra as measured directly as well as corrected for this amount of reddening using the extinction corrections of Cardelli, Clayton, & Mathis (1989), including the O'Donnell (1994) modifications at blue wavelengths.

3.4. *Line Measurements*

The emission-line intensity ratios of the late-time spectra of SN 1993J are fairly difficult to measure. The large velocity width of the lines (FWHM $\gtrsim$ 15000 km s^{-1}; see, e.g., Figs. 7, 8, 10, 11, 12, and 13 of Paper I and below) and consequent overlapping make the deblending of the lines almost impossible. Without a clean, isolated line to provide a well-defined profile, all measurements will be affected by a relatively large uncertainty. Despite this problem, we were able to extract some information from the spectra.

The first step in the line measurement was the removal of the underlying "continuum." This is not an actual contin-

uum from a photosphere, but rather a mixture of blended lines that combine to produce a relatively smooth pseudo-continuum, extending from the ultraviolet (UV) edge of our spectra to ~ 5500 Å. (The pseudo-continuum was removed over the entire range of our spectra; redward of 5500 Å it is much weaker.) The circumstellar interaction itself can also produce a weak blue continuum (Fransson 1984). The stronger region of the pseudo-continuum is probably iron and iron-group element emission. Beyond 5500 Å, these species also contribute, but there may be other sources responsible for the red light. As this is not a well-defined continuum, its removal is an additional factor in the uncertainty of any measurements. The subtraction of the pseudo-continuum was accomplished with a spline fit by hand to the spectra, but in a consistent manner for all of the spectra to be analyzed.

Line fluxes were calculated by summing the contributions from each pixel over a range determined by the best approximation of the edges of the line. In the cases of blended lines, total fluxes were measured. The edges of the lines provided the values for the maximum blue and red velocities for the given line(s). Table 1 lists the fluxes of the lines available in our spectra relative to Hα, with the second number indicating the line ratios when dereddened by $A_V = 0.6$ mag. The relative spectrophotometry of the spectra is excellent (see Paper I for discussion of the observing and calibration details), so the major sources of uncertainty in the fluxes are line blending, choice of line boundaries, and the subtraction of the continuum. The relative flux values probably have uncertainties of $\sim 10\%$; individual measurements with larger uncertainties are denoted in Table 1. Table 2 reports the velocities of the lines determined from the same measurements; similar caveats about the uncertainties of the fluxes apply to the velocities, although the values for FWHM are more secure than either the blue velocity at zero intensity (BVZI) or the red velocity at zero intensity (RVZI).

For the day 976 spectrum (see Fig. 10), we felt that the line shapes were sufficiently simple and well-defined compared to the other epochs to attempt a decomposition of the He I λ5876 + Na I D blend. We modeled the line as a simple box shape with an appropriate velocity width (15,000 km s^{-1}). Using the SPECFIT task in the STSDAS package of IRAF, we found a good fit to the blend with approximately

TABLE 1

RELATIVE LINE FLUXES

Day[a]	Hα, λ6563	He I λ5876+ Na I λλ 5890, 5896	[O I] λλ6300, 6364	[O II] λλ7319, 7330	[O III] λλ4959, 5007 +Hβ λ4861	[O III] λ4363	[Ne III] λ3967
553	100, 100	30, 32	8.8, 9.0	23, 21	33, 39	34, 44	45, 62
670	100, 100	29, 30	4.9, 5.0	23, 21	29, 35	27, 35	...
881	100, 100	40, 43	4.6, 4.6:	...	37, 44:	...	...
976	100, 100	37, 39	3.2, 3.3	25, 23	33, 40	27, 35	...
1766...	100, 100	54, 57	6.8, 6.9	46, 44	40, 48	19, 25	...
2028...	100, 100	82, 86:	18, 18:	85, 80:	80, 94:	33, 44:	62, 85:
2069...	100, 100	90, 95	12, 12:	52, 50	87, 104	27, 36:	73, 100:
2115...	100, 100	66, 70	12, 12	68, 65	79, 94	28, 36:	72, 100:
2176...	100, 100	70, 74	16, 16:	71, 67	67, 80	30, 39	96, 132:
2454...	100, 100	74, 78	13, 13	89, 84	76, 91	24, 31	...

NOTE.—Listed relative to Hα ≡ 100. First value is relative flux as directly measured; second value is relative flux corrected for a reddening of $A_V = 0.6$ mag using the extinction corrections of Cardelli et al. (1989), including the O'Donnell (1994) modifications. In all cases a continuum was removed from beneath the individual lines. When two (or more) lines are listed, the flux indicated is the sum for all. Values are uncertain by $\sim 10\%$ (those indicated with a colon are uncertain by $\gtrsim 20\%$).

[a] Day since explosion, 1993 March 27.5 UT.

TABLE 2

MEASURED VELOCITIES

Day[a]	Hα, λ6563 BVZI[b]	Hα, λ6563 BVZI[b]	Hα, λ6563 FWHM[b]	Hβ, λ4861 BVZI[b]	[O III] λ5007 RVZI[b]	He I λ5876 BVZI[b]	Na I λ5890 RVZI[b]
433	−16600	11700	23100	...	...	...	...
473	−16100	10900	22000	...	...	...	...
523	−10400	13100:	17400	...	...	...	...
553	−10000	9800	17200	−10500	9100	−16200	8400
670	−10500	10100	16900	−9700	9600	−16000	9200
881	−10300	9500	16400	−9500	10000	−16200	8700
976	−10600	9800	16000	−9500	8000	−16000	8900
1766.....	−9900	9700	15000	−9700	7600:	−15600	8500
2028.....	−8900	9100	15000	−10400	9800	−21100:	8400
2069.....	−9400	9100	15000	−12000	7500	−17200	8700
2115.....	−9900	9300	14700	−14900:	7200:	−15400	8300
2176.....	−9600	9000	14900	−11800:	6700:	−15900	7700
2454.....	−9300	8700	13800	−13400:	8400:	−15200	7500

NOTE.—All velocities are km s^{-1}. Values are uncertain by $\sim 10\%$ (those indicated by a colon are uncertain by $\sim 20\%$–30%).

[a] Day since explosion, 1993 March 27.5 UT.

[b] BVZI = blue velocity at zero intensity; RVZI = red velocity at zero intensity; FWHM = full width at half maximum.

equal contributions from both He I λ5876 and Na I D (Fig. 11). Later spectra were either too noisy or did not show as clean a box shape for the profile as did the day 976 spectrum. Visual inspection of the later spectra, however, indicates that the relative ratio of these two lines does not appear to change significantly. This can be seen in Figure 10 of Paper I. The blue edge of He I λ5876 and the red edge of Na I D are not as sharp in later spectra as they are on day 976. For days 2028 to 2176, the lower S/N is at least partly responsible for degrading the line profile. By day 2454, though, the edges still appear, but the shoulders of the lines are more rounded. This may indicate that the spherical structure that produces the boxlike profiles is beginning to lose its coherence. When comparing the relative heights of the blue and red shoulders of the He I λ5876 + Na I D blend, one must consider that the pseudocontinuum affects the blue half more than the red. Taking this into account, the relative strengths of the two lines appear to remain effectively constant. There may be a slight increase of the strength of He I λ5876 in comparison with Na I D, but it is not a significant change. Therefore, the line ratio for the He I λ5876 + Na I D blend reported in Table 1 can probably be interpreted as approximately half He I λ5876 and half Na I D.

We also employed a decomposition technique that used one of the lines in the spectra to model the others. The individual species were different enough that we chose to use the line of a given element to isolate only lines from the same species, although different ionization states were allowed. Given the lines available, this restricted us to the use of Hα to model Hβ, and [O II] $\lambda\lambda$7319, 7330 to model [O I] $\lambda\lambda$6300, 6364 and [O III] $\lambda\lambda$4959, 5007. The line used as the model was isolated from the spectrum, shifted in wavelength space to match the other line, and then scaled until the subtraction of the model gave the most effective removal of the other line. The choice of scaling was subjective, as contamination by other species and noisy spectra precluded a more formal comparison. (The [O I] $\lambda\lambda$6300, 6364 doublet was removed from the blue edge of Hα before it was used.) The fact that [O II] $\lambda\lambda$7319, 7330 matched the other oxygen lines so well suggests that there is very little, if any, contamination by [Ca II] $\lambda\lambda$7291, 7324 in this wavelength region at late times. Calcium is probably the more significant line at earlier times, as discussed in § 2. The relative line fluxes determined with this technique are reported in Table 3. The line-subtraction technique was only effective in the spectra from day 976 onward. In addition, the results were more accurate for the high S/N spectra from Keck (days 976, 1766, and 2454) than for the more noisy spectra from Lick (days 2028, 2069, 2115, and 2176).

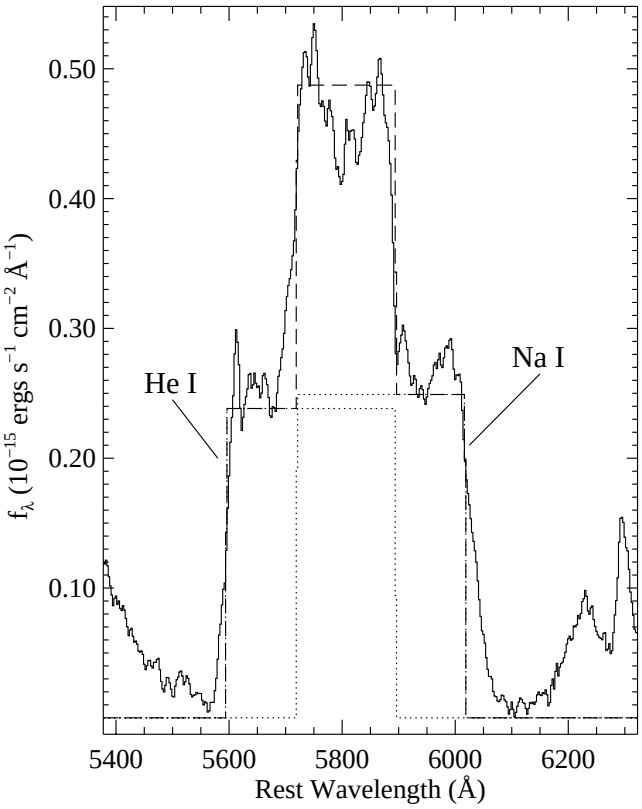

FIG. 11.—Decomposition of the He I λ5876 + Na I D blend on day 976 using simple boxlike profiles to model the individual lines. The dotted lines indicate the two separate components (He I λ5876 and the Na I D blend), while the dashed line is the sum that produces the overall blend. This best fit indicates that the two lines contribute approximately equally to the blend.

3.5. *Discussion*

Most of our interpretation of the late-time spectra of SN 1993J falls within a comparison with the circumstellar interaction model of CF94. The CF94 model envisions cool, freely expanding SN ejecta colliding with circumstellar material from a preexplosion stellar wind. A forward shock propagates into the wind, while a reverse shock moves back into the ejecta. The SN ejecta have a fairly steep density gradient, leading to a slow reverse shock with emission at far-UV wavelengths (possibly in X-rays, with a different gradient). This produces emission from highly ionized species. Absorption by a shell formed at the shock boundary can yield low-ionization lines, although these can also originate in the ejecta themselves. CF94 treat two different models for the structure of the wind. One is a power law, most applicable to a relatively compact progenitor, while the other uses the density structure of a red supergiant (RSG) from stellar evolution models. They make specific predictions for their model, including line intensity ratios and line profiles.

TABLE 3

LINE DECOMPOSITION FLUXES

Day[a]	Hβ[b] λ4861	[O I][c] λ6300	[O III][c] λ5007
976	0.2, 0.3	0.3, 0.3	1.5, 1.9
1766.....	0.2, 0.2	0.3, 0.3	1.3, 1.6
2028.....	0.3, 0.4	0.3, 0.4	1.3, 1.8
2069.....	0.3, 0.4	0.4, 0.4	1.9, 2.3
2115.....	0.2, 0.3	0.3, 0.3	1.5, 1.8
2176.....	0.2, 0.3	0.3, 0.4	1.4, 1.7
2454.....	0.1, 0.1	0.3, 0.3	1.2, 1.4

NOTE.—Line fluxes as a fraction of another line in the spectrum. Details of decomposition are presented in the text. The first number is the fraction as measured; the second is the fraction after the spectrum has been dereddened by $A_V = 0.6$ mag using extinction corrections of Cardelli et al. (1989), including the O'Donnell (1994) modifications. The values for days 2028, 2069, 2115, and 2176 are much less certain than those for days 976, 1766, and 2454.

[a] Day since explosion, 1993 March 27.5 UT.

[b] Fraction relative to the strength of Hα.

[c] Fraction relative to the strength of [O II] $\lambda\lambda$7319, 7323.

3.5.1. *Velocities*

The uncertainty of the edges of the lines at zero intensity, as well as the large number of potentially overlapping lines, makes interpretation of the measured velocities problematic. One of the very specific predictions of CF94's interaction model is that the line widths decrease with time. A pulsar-powered model would have velocity widths that *increase* slowly with time, and would have $v \lesssim 1000$ km s^{-1} (Chevalier & Fransson 1992). The velocities listed in Table 2 appear to suggest a general decrease over time. The Hα BVZI is severely contaminated by [O I] $\lambda\lambda$6300, 6364 at early times, and this contamination never completely vanishes. In addition, Hα may be affected on the red side by He I λ6678. Given that He I λ5876 is approximately one-third the strength of Hα (see Table 1 and § 3.4), He I λ6678 probably only has a small effect on Hα, unless unusually high densities are altering the typical He I line intensity ratios (e.g., Almog & Netzer 1989). The RVZI for [O III] $\lambda\lambda$4959, 5007 is difficult to isolate, and thus is highly uncertain. The BVZI for Hβ appears to grow fairly dramatically at late times, but this is more likely the result of contamination by another species than any change in Hβ itself. A comparison of Hα and Hβ in velocity space on day 1766 and day 2454 (Fig. 12), though, shows that the blue edge of Hβ does not look like Hα at late times and is probably some other species. The CF94 model does predict a strong Mg I] λ4571 line, but this feature near Hβ is at the wrong wavelength to be magnesium.

The BVZI of He I λ5876 and the RVZI of Na I D are more likely to reflect the actual limits of velocity space occupied by their respective species. The most accurate velocity information comes from the FWHM of Hα. This is much less affected by errors in the subtraction of the pseudo-continuum, and there is less impact by weaker lines. There is still some contamination by [O I] $\lambda\lambda$6300, 6364, but the line-subtraction technique described above indicates that it widened Hα minimally. Perhaps the best evidence that the FWHM of Hα is fairly accurate is how remarkably constant the values are. Probably from day 881, and definitely from day 1766, the FWHM is $\sim$15,000 km s^{-1}, within our measurement uncertainty. The decrease found by day 2454 appears to be real. If this is the case, then the line widths are decreasing in accordance with the CF94 model. Marcaide et al. (1997) also found an apparent deceleration in the ejecta using very long baseline interferometry.

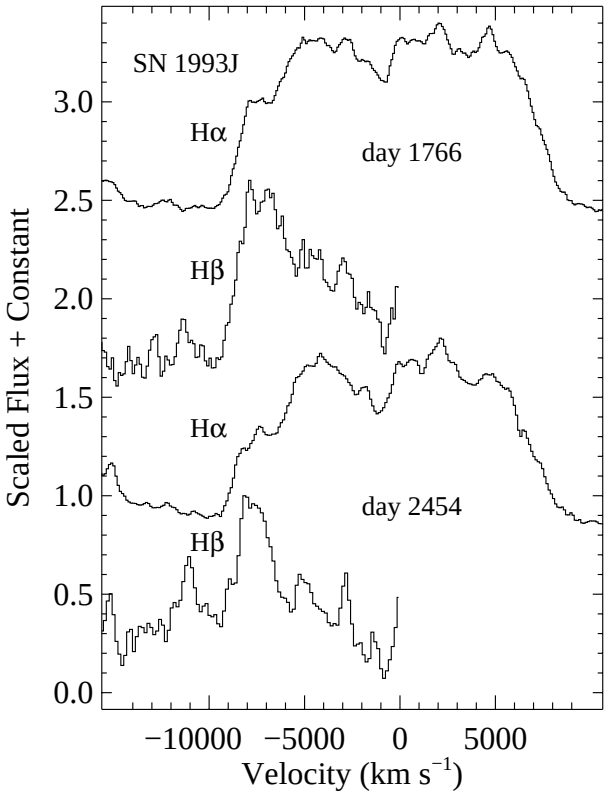

FIG. 12.—Comparison of the Hα and Hβ lines on days 1766 and 2454. The red half of Hβ is heavily contaminated by [O III] $\lambda\lambda$4959, 5007, so it has been removed for clarity. The relatively strong, narrow Hβ feature at about -8000 km s^{-1} does not appear to correspond with the structure of Hα, which is contaminated by [O I] $\lambda\lambda$6300, 6364 on the blue side (see Fig. 13).

The CF94 model has other predictions relevant to the observed velocities. One is that highly ionized lines should have different velocity widths than low-ionization lines. Unfortunately, we cannot test this predication, as the difference is only $\sim$830 km s^{-1} in the power-law model for the wind structure. Another is the scale of the line-profile widths. In the power-law model, the half width at zero intensity (HWZI) is $\sim$5000 km s^{-1}, while for the RSG model, the HWZI is $\sim$4200 km s^{-1}. For the lines of SN 1993J, the HWZI is $\sim$7500 km s^{-1}. This is not surprising as the structure of the progenitor of SN 1993J would not have been that of a typical RSG. It may indicate that the particular power law used is not applicable to SN 1993J either. The four SNe discussed by F99 (1986E, 1980K, 1979C, and 1970G) have expansion velocity widths (HWZI) on the order of 5500 km s^{-1}, implying that they have higher mass envelopes than SN 1993J. This is understandable, as most models for SN 1993J postulate that it had a low-mass (0.2–0.5 $M_\odot$) hydrogen envelope, so a smaller mass implies a larger velocity for a given amount of input energy (see Paper I and references therein). In all five cases, though, the velocities are larger than predicted by any of CF94's models. In addition, the mass-loss rate of SN 1993J as determined from radio observations (Van Dyk et al. 1994) is (2–15) $\times$ 10^{-5} $M_\odot$ yr^{-1}, and this is comparable to the values for the other four SNe [(2$-$19) $\times$ 10^{-5} $M_\odot$ yr^{-1}; F99 and references therein].

3.5.2. *Emission Lines*

Table 4 lists the predicted line fluxes from the CF94 model, both for the power-law wind structure and the RSG model. The measured fluxes from our data range from 1.8 to 6.7 yr, thus providing a comparison with several epochs of the model. Table 4 only contains the lines with which we can make any comparisons. The limitations of the spectra in wavelength coverage and quality at red wavelengths restrict the set of usable lines. The blending of the lines also complicates some direct comparisons.

The spectra from days 653, 670, 881, and 976 are closest to the CF94 year 2 predictions. For these days, assuming Na I D is half the blend of He I λ5876 + Na I D as described above, the sodium line is nearly half the predicted strength. The [O I] $\lambda\lambda$6300, 6364 doublet is only a quarter of the predicted value and [O II] $\lambda\lambda$7319, 7330 is three times stronger than in the model, but the [O III] $\lambda\lambda$4959, 5007 strength may be comparable. If the line subtraction technique is correct, and Hβ is 0.2–0.3 of the Hβ + [O III] blend, then the observed oxygen-line flux is similar to the predicted value. Unfortunately, the [Ne III] λ3968 line was

TABLE 4

PREDICTED LINE FLUXES

Age (yr)	Hα λ6563	Hβ λ4861	[O I] λλ6300, 6364	[O II] λλ7319, 7330	[O III] λλ4959, 5007	[Ne III] λλ3868, 3969	Na I D λλ5890, 5896
PL:[a]							
1.....	100	14	26	3	7	11	27
2.....	100	23	26	6	27	18	38
5.....	100	30	35	14	100	30	61
10.....	100	32	52	15	220	43	100
17.5.....	100	34	72	14	470	55	140
30.....	100	34	74	12	640	56	140
RSG:[b]							
10.....	100	33	14	...	340	30	17

NOTE.—Line fluxes from the circumstellar interaction model of Chevalier & Fransson (1994), listed relative to Hα ≡ 100. Only the lines relevant to our observations are shown.

[a] Power-law model.

[b] Red supergiant model.

not available in all our spectra. Its value on day 653 is three times larger than predicted, but this region has the most uncertainty due to potential line contamination and the decreasing quality of the spectra toward blue wavelengths.

The later spectra are closer in time to the year 5 model of CF94, but we will also consider the year 10 models. The Na I D strength is still weaker than predicted, but closer to calculated values, and would actually fit well with the prediction for year 2. The relative strength of the sodium line does increase, as is the general trend in the models. The RSG model actually predicts a quite low value for Na I D, in contrast to the power-law model. While continuing to gain in relative strength, [O I] λλ6300, 6364 is still far below the predicted values for the power-law model. In this case, the oxygen doublet is in agreement with the RSG value at year 10. The biggest difference between the observations and the models may be the strength of [O II] λλ7319, 7330. In the models, this feature barely contributes, while the observations show it to be a significant line, with 70%–80% of the strength of Hα. Unfortunately, the CF94 RSG model does not report the predicted strength of [O II] λλ7319, 7330. The RSG model predicts an even higher strength for [O III] λλ4959, 5007 relative to Hα than the power-law model, and this is not what is observed, so we will concentrate on the predictions of the power-law model.

As [O II] λλ7319, 7330 is expected to originate in the ionized ejecta along with [O III] λλ4959, 5007, it is unclear why the singly ionized oxygen lines should be so strong, when the doubly ionized lines are slightly weaker than the models indicate unless the ionization structure is fairly different from the models' assumptions. The density may explain the ratios, as will be discussed below. Chevalier & Fransson (1989) show that [O II] λλ7319, 7330 is stronger in models of typical late-time spectra of core-collapse SNe without circumstellar interaction. Unfortunately, [Ca II] λλ7291, 7324 is predicted to be an order of magnitude stronger than the [O II] lines, so the circumstellar model is more appropriate, although the depletion of calcium onto dust grains formed as the ejecta cool may affect the [Ca II] λλ7291, 7324 line strength (e.g., Kingdon, Ferland, & Feibelman 1995).

The [Ne III] λ3968 line is again uncertain in these very late-time spectra, but it appears to be significantly stronger than the models predict. This makes the issue of ionization structure even more complicated, as this high-ionization line also originates in the ejecta. If the relative strengths of [O II] and [O III] are the result of a lower ionization of the ejecta, then the strength of [Ne III] is difficult to explain. This may imply that there are also abundance issues that affect the relative line strengths. As SN 1993J was assumed to have lost most of its hydrogen envelope (see Paper I and references therein), perhaps the relative amount of hydrogen has been depleted in the ejecta compared to the abundances used in CF94's models, which were computed for normal SNe II. This could explain the apparent excess of emission from the lines that originate in the ejecta ([O II], [Ne III]), while the lines that originate in the shell (Na I D, [O I]) seem too weak, as all the line ratios are relative to Hα. The strength of [O III] actually fits with the predictions, and thus does not necessarily support this scenario.

Some of the lines predicted by CF94 are notable by their absence from our spectra. These include [C I] λ8729, [N II] λλ6548, 6583, [O II] λλ3726, 3729, Mg I] λ4571, and [S III] λλ9069, 9532. The carbon line would not be particularly strong, but the near-IR sulfur lines would be comparable in strength to Hα. Neither of these features is apparent, although hints of the sulfur line may exist in the day 2176 spectrum (Fig. 10 of Paper I), but clearly at a lower strength. The [O II] λλ3726, 3729 line could be contributing to the [Ne III] λ3968 line, but the distinctive double-horned oxygen line profiles described below do not appear and the wavelengths do not match well. As discussed above, the Mg I] λ4571 line might be appearing at the blue edge of Hβ, but the velocities are not correct. In addition, the magnesium line should be two-thirds of the strength of Hα, and that is obviously not the case. The nitrogen lines could be hidden within the Hα structure, but there should then be a shoulder on the blue edge of Hα caused by the λ6548 component. The predicted total [N II] λλ6548, 6583 flux is about one-third that of Hα, and if the line ratios are not affected by density considerations, then the λ6548 line may be too weak to show up on the Hα profile. As we show below, there is contamination on the blue side, but from [O I] λλ6300, 6364.

Most of these apparently missing lines have one attribute in common—a low critical density. For [O II] λλ3726, 3729, [N II] λλ6548, 6583, and [S III] λλ9069, 9532, the critical densities are all less than 10^6 cm^{-3} for $T \approx 10{,}000$ K. (These, and subsequent values for the critical density and other line diagnostics, were calculated with the IRAF/STSDAS NEBULAR suite of tasks.) The [C I] λ8729 line has a high critical density ($>10^7$ cm^{-3}), so its absence,

along with the lack of Mg I] λ4571, may be explained by an origin in the shell, whose lines appear to be weaker than those from the ejecta. The critical density for [O II] $\lambda\lambda$7319, 7330 at $T \approx 10{,}000$ K is 5.7×10^6 cm^{-3}, while it is only 6.2×10^5 cm^{-3} for [O III] $\lambda\lambda$4959, 5007. This may explain the relative weakness of [O III], if the absence of the other lines does imply a density $\gtrsim 10^6$ cm^{-3}.

The [O III] lines may be able to further constrain the density. The [O III] λ4363 and $\lambda\lambda$4959, 5007 lines are contaminated by Hγ and Hβ, respectively. This contamination is potentially significant from days 553 to 1766, but probably less than 20% thereafter (see Tables 1 and 3). The relative contamination of Hβ would be greater, and this would tend to drive the [O III] ($\lambda\lambda$4959, 5007/λ4363) ratio lower as it dilutes [O III] $\lambda\lambda$4959, 5007 if removed properly. Residual Hβ contamination could drive the [O III] ($\lambda\lambda$4959, 5007/λ4363) ratio higher. Without considering the effects of the hydrogen lines, though, the [O III] ($\lambda\lambda$4959, 5007/λ4363) ratio is already ~ 1 at day 670, implying that, to within the uncertainties of our measurements, we can probably ignore the hydrogen without affecting our interpretation significantly. To get [O III] ($\lambda\lambda$4959, 5007/λ4363) as low as 1, the temperature must be at least 10,000 K, even at the large densities considered here. The electron density under these conditions would be $n_e \gtrsim 10^8$ cm^{-3}. By day 2454, the ratio is $\sim$3, implying a density of $n_e \approx 10^7$ cm^{-3}. For higher temperatures, the required density drops. If $T \approx 30{,}000$ K, for example, $n_e \approx 10^7$ cm^{-3} on day 670 and $n_e \approx 2 \times 10^6$ cm^{-3} by day 2454. No matter what the temperature is, the increase of the [O III] $\lambda\lambda$4959, 5007 to λ4363 ratio with time implies a decreasing density, as one would expect in the expanding ejecta. Given the discussion of critical densities above, a density $\gtrsim 10^6$ cm^{-3} with a temperature of $T \approx 10{,}000$–$30{,}000$ K appears to be consistent with the line emission.

The relative ratios observed are, for the most part, consistent with values determined by F99 from other late-time spectra of core-collapse SNe. Both SN 1980K and SN 1979C have very similar line ratios when compared with SN 1993J. This includes the large amount of emission in [O II] $\lambda\lambda$7319, 7330. SN 1986E has a much weaker [O II] feature (see also Cappellaro et al. 1995; they identify the line at $\sim$7300 Å as the [Ca II] $\lambda\lambda$7291, 7324 doublet). SN 1979C is the only one of these four to have a measured [Ne III] λ3968 line, and it is not as strong as in SN 1993J. The lines predicted by CF94 that are missing in SN 1993J are also missing in these SNe, suggesting that they, too, have a density higher than the critical density of these lines.

A few of the late-time spectra were observed on photometric nights. For these, we calculated the luminosity of the Hα line using a distance to M81 of $d = 3.6$ Mpc (Freedman et al. 1994). On days 553, 670, and 881, the Hα luminosity was (in units of 10^{38} ergs s^{-1}) 2.5, 3.0, and 4.8, respectively. By day 1766, it was 0.86, and 0.37 on day 2454. (To correct for an extinction of $A_V = 0.6$ mag, the luminosities would be multiplied by 1.5.) Both the day 553 and day 670 spectra were observed through relatively narrow slits on nights with variable seeing, implying a larger uncertainty for the luminosities calculated for those observations. The day 881 spectrum was taken with a 4″ slit width; thus, the value of 4.8×10^{38} ergs s^{-1} is probably a better indication of the Hα luminosity during these days. Note that FMB94 found the luminosity of the Hα line to be 4.4×10^{38} ergs s^{-1} on day 433—a comparable value within our probable uncertainties. The day 1766 and day 2454 spectra were also taken through narrow slits, with the seeing comparable to the slit width. Therefore, the luminosities at these later times could be larger (or smaller) than measured, but most likely by not more than a factor of two, implying a real decrease in Hα luminosity by such late times. CF94 predicted an Hα luminosity of 0.45, 0.19, and 0.09×10^{38} ergs s^{-1} at 2, 5, and 10 yr, respectively, for the power-law model. The RSG model gave an Hα luminosity of 0.48×10^{38} ergs s^{-1} at 10 yr. Patat et al. (1995) found an Hα luminosity of 1.3×10^{38} ergs s^{-1} (corrected for extinction of $A_V = 0.1$ mag) on day 368 (their day 367) and they interpreted this level of emission as a requirement for circumstellar interaction; radioactive decay alone was not enough. Our values are consistent with the Patat et al. (1995) model that requires circumstellar interaction to power the emission. The luminosities we observe at late times for SN 1993J agree with the values reported for other SNe observed at similar times (see F99 for a table of values).

3.5.3. *Overall Comparison with the Circumstellar Interaction Model*

The CF94 model makes many predictions for the spectrum resulting from circumstellar interaction. The comparison of these predictions with the late-time spectra of SN 1993J and the prior study of F99 indicates that the model is somewhat successful, but needs refinement. The velocity widths in SN 1993J and the four SNe of F99 are larger than the model predicts, especially larger than those of the RSG model, but they do follow the expected trend of a general decrease with time. The line intensity ratios of the RSG model seem fairly inconsistent with the observed values. The power-law model is slightly better, as the trends of the relative ratios over time are consistent. One exception to this is the prediction of a strengthening of Hβ relative to Hα as the interaction continues; we do not see this in SN 1993J (see Tables 3 and 4), although the density of the emitting material may affect this result. The trend of a decreasing luminosity for the Hα line at late times is also consistent between the observations and the models, although the absolute values differ.

The power-law model predictions may not be so different from the observed results if density effects are considered. Many of the emission lines predicted by the model that have low critical densities are absent from the spectra of SN 1993J and the four SNe discussed by F99. SN 1993J may have a relatively lower hydrogen abundance, as shown by its transformation from Type II to Type IIb. This will increase the relative intensity of other lines. The fact that similar values are seen in the four SNe of F99, though, implies that the low-mass envelope of SN 1993J is not altering the circumstellar interaction significantly. A larger density for the emitting region associated with the circumstellar interaction may be the main explanation for the deviation of the line intensity ratios from the predictions of the CF94 models. The relative weakness of lines predicted to arise in the ejecta, as opposed to the shell, argues that a depleted level of hydrogen may have some impact on the line-intensity ratios.

3.5.4. Hα *Line Structure*

One other aspect of the late-time Hα line is that it shows a persistent, narrow (unresolved, FWHM $\lesssim 250$ km s^{-1} on day 1766) feature at zero velocity (see Fig. 9 for a detailed view on day 433). Careful inspection of Figure 10 shows

that the line is present in all three of the high S/N, late-time spectra. It is not clear if this is emission from flash-ionized circumstellar material around SN 1993J (as noted in early spectra, see Paper I and references therein), or merely an H II region along the line of sight. Finn et al. (1995) noted the presence of this feature and found it to be slightly variable in strength. They also show (their Fig. 7) an image of the environment of SN 1993J taken through a narrowband filter centered on Hα. There is faint H II region emission evident around the SN. Aldering, Humphreys, & Richmond (1994), while studying earlier images of M81 to analyze the progenitor of SN 1993J, found that the colors indicated more than one star, and perhaps a faint OB association, that could be the source of the narrow hydrogen emission. Finn et al. (1995) concluded that the feature was probably not directly connected with SN 1993J. If the emission is not associated with SN 1993J itself, then it cannot originate very far from the line of sight to SN 1993J. Data from the Keck telescope on day 1766 were taken through a 1″ slit with ∼1″ seeing (the extraction width was 4.″2). The narrow feature is still present, and thus is likely directly along the line of sight. The Hβ line shows no evidence for this feature, but the S/N of the spectra in this region would make identification difficult.

Another possible source for the narrow Hα line is material ablated from a companion star. As discussed in Paper I, many models for SN 1993J postulate a companion to facilitate the loss of the hydrogen envelope from the progenitor. Chugai (1986), Livne, Tuchman, & Wheeler (1992), and Marietta, Burrows, & Fryxell (2000) have considered the effects of the interaction of a SN explosion with a companion. Their calculations indicated that material from a companion to an exploding white dwarf could be swept up in the ejecta with emission becoming visible several hundred days after the explosion. The predicted widths, though, range from a few hundred to over a thousand kilometers per second. Given the low velocity width of the observed late-time narrow Hα line in SN 1993J, it is unlikely that ablated material from the companion star is the source.

As can be seen in Figure 10, there are small-scale features covering the flat top of the Hα profile similar to the clumps described in § 2 for the oxygen lines. In this case, though, the structures change over time. As noted by FMB94, they probably represent Rayleigh-Taylor instabilities in the hydrogen-emitting region behind the shock (Chevalier, Blondin, & Emmering 1992). The instabilities are enhanced if the shock is radiative (Chevalier & Blondin 1995), as Fransson et al. (1996) suggest for SN 1993J.

3.5.5. *Late-Time Oxygen Lines*

The relative strengths of the various oxygen lines are shown by the ratios determined using the line-subtraction technique described in § 3.4 and presented in Table 3. The [O I] λλ6300, 6364 to [O II] λλ7319, 7330 ratio is approximately constant. The values for the ratio of [O III] λλ4959, 5007 to [O II] λλ7319, 7330 are difficult to interpret given their apparently large and random range. The values from the Keck spectra (days 976, 1766, and 2454) are the most reliable, and, considering only these values, the relative strength of [O III] λλ4959, 5007 appears to weaken slightly compared with [O II] λλ7319, 7330 over the course of the observations. This may indicate a reduction in the strength of the interaction and thus a decrease in the ionization level within the ejecta. Given the uncertainty in these values, this is highly speculative.

A striking change occurs in the spectra of SN 1993J between days 976 and 1766. The oxygen lines ([O I] λλ6300, 6364, [O II] λλ7319, 7330, and [O III] λ4363 and λλ4959, 5007) all develop narrower profiles on top of the underlying boxlike shape (see Fig. 10). These features are not contamination by other lines, as they appear with the same relative velocities for all of the oxygen lines accessible in our spectra (Fig. 13). The peaks of the narrower profiles are separated by ∼7100 km s^{-1}, so these are not the two components of the oxygen doublets (the maximum velocity separation for the oxygen doublets is ∼3000 km s^{-1} for [O I] λλ6300, 6364). We believe that these profiles represent the blue and red peaks of a double-horned profile due to the ejecta colliding with a disklike, or at least a somewhat flattened, region. (For a derivation of the two-horned profile from an expanding disklike structure, see, e.g., Leonard et al. 2000; Gerardy et al. 2000.) The disklike structure may be due to the interaction of circumstellar material with a binary companion, thought to be present according to models for mass loss from the progenitor of SN 1993J (see Paper I and references therein). The red horn is weaker than the blue horn due to differential extinction; we see the former through a much longer path in the ejecta. The large gap in our coverage between days 976 and 1766 means that the onset of the

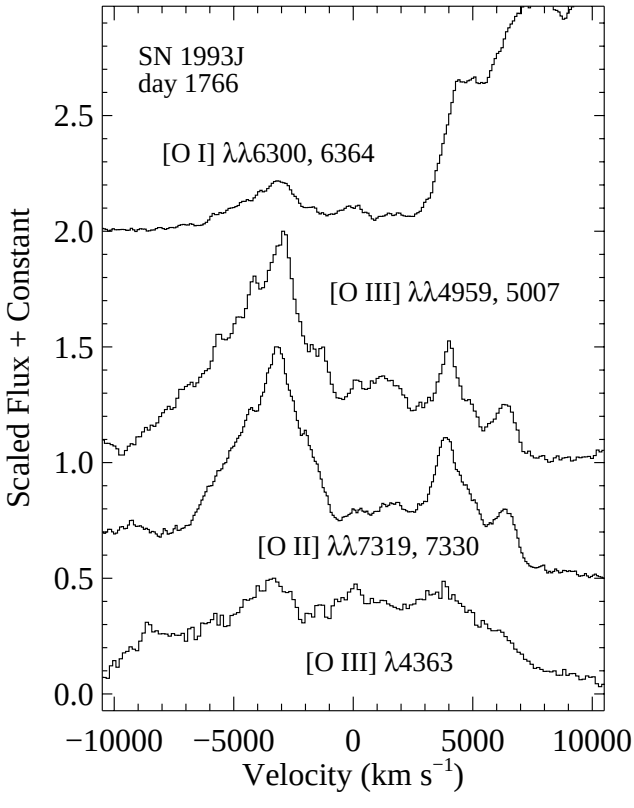

FIG. 13.—Four oxygen lines on day 1766. The two-horned structure is clearly evident for [O II] λλ7319, 7330 (zero point: 7325 Å) and [O III] λλ4959, 5007 (zero point: 5007 Å). The weakness of the lines, contamination from other species, and the noisy nature of their regions of the spectra obscure the features in [O III] λ4363 and [O I] λλ6300, 6364 (zero point: 6300 Å), but they are still apparent. The red peak of [O I] λλ6300, 6364 is visible as a distinct shoulder on the blue side of Hα. The consistency of the two-horned structure over several lines, as well as the large velocity separation of the two horns (∼7100 km s^{-1}), indicates that these profiles do not represent the two separate components of any of the oxygen doublets, but rather show the presence of a flattened, disklike structure.

disk features was not recorded. There are vague hints of the incipient two-horned structure on day 976 (Fig. 14), but it is certainly not as significant as in the later spectra. This type of structure is not evident in any of the four SNe whose late-time spectra are discussed by F99.

Starting with the day 1766 spectrum, a notch develops in the middle of the Hα line. This loss of flux at zero velocity may indicate a slight flattening of the spherical distribution that had been the source of the hydrogen emission. Blondin, Lundqvist, & Chevalier (1996) present a model for an axisymmetric circumstellar interaction in which the SN is interacting with a dense equatorial structure. Such a scenario would result in little emission along the axis of symmetry because of a lower abundance of circumstellar material, while the equatorial structure would emit as in a typical interaction. This could create a disklike or flattened source of circumstellar emission as is seen here. As the ejecta expand, they can interact with the disklike or flattened circumstellar material producing the two-horned profiles. The emission-line profile from an expanding disk is double peaked and resembles that of a bipolar ejection. In fact, some new models for the core-collapse mechanism may require a bipolar outflow (Khokhlov et al. 1999), although they are fairly speculative. In addition, the optical spectropolarimetric studies of SN 1993J indicated asymmetries at early times (Trammell, Hines, & Wheeler 1993; Tran et al. 1997). Polarimetry of other SNe (e.g., Leonard et al. 2000; Wang et al. 2000) also suggests that asymmetries might be common, although the late appearance of a nonspherical emission source may indicate that the circumstellar matter is the cause of the asymmetry.

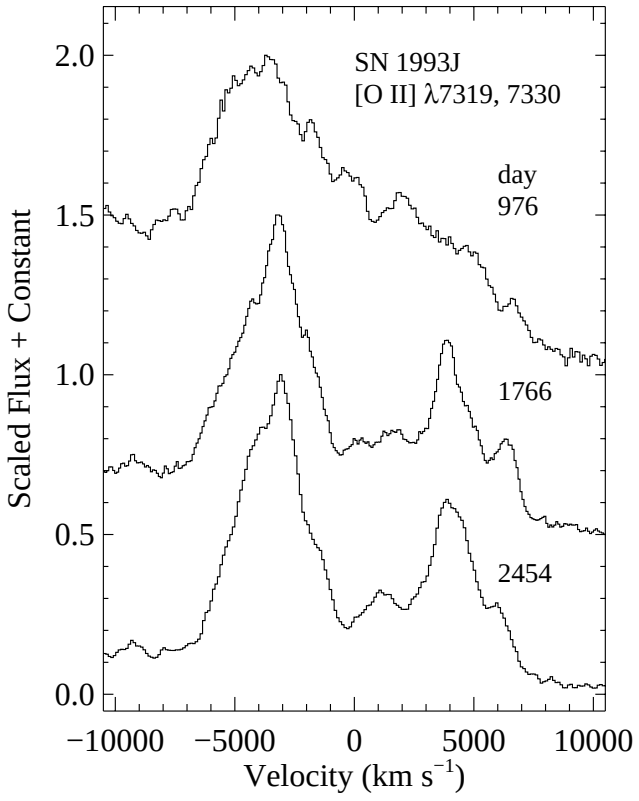

FIG. 14.—Line profiles of [O II] λλ7319, 7330 on 976, 1766, and 2454. The zero point for the velocity is 7325 Å. The two-horned structure is obvious in the last two spectra, but the beginnings are apparent even at day 976, especially for the blue peak.

The appearance of this disklike structure may complicate the interpretation of the line-intensity ratios discussed above. There is still the boxlike profile from a roughly spherical source, in addition to the flattened region. The discussion of line ratios assumed that the conditions were the same for the entire emitting region. It may be that the shell and the disk have distinctly different physical conditions, but such differences would be very difficult to separate in our spectra. The wings of the disklike profile are obvious, but the precise decomposition of the line into disk and shell components would be model dependent. This is made even more complicated by the fact that the boxlike profile shows no significant asymmetry, while the two-horned profile is clearly stronger in the blue component. This implies that the flattened region suffers from differential extinction, while the roughly spherical shell does not.

4. CONCLUSIONS

The detailed substructure of the ejecta revealed by the spectra from early to nebular times indicates that SN 1993J is a clumpy supernova. (For a discussion of substructure that is the result of telluric absorption, see the Appendix.) Both oxygen and magnesium lines show clumps. The oxygen clumps appear in both permitted and forbidden lines, with some slight variations. The calcium lines do not seem to have clumps. This is consistent with a scenario in which the observed oxygen emission originates in clumps of the newly synthesized material (either through prior evolution or explosive nucleosynthesis), while the calcium emission arises mostly from preexisting material distributed uniformly throughout the envelope, following the models of Li & McCray (1992, 1993). Using the technique of Chugai (1994), we find a total oxygen mass based on the observed clumps of $M_{\rm O} \approx 0.7$–$0.9\ M_{\odot}$. This value is very uncertain and it is larger than the values predicted by models of SN 1993J.

We also present late-time spectra of SN 1993J. The lines clearly exhibit circumstellar interaction through their boxlike emission profiles. They indicate a gradual decrease in velocity width from day 433 to day 2454, with the FWHM of Hα remaining relatively constant from day 976 to day 2176 at $\sim$15,000 km s^{-1}, decreasing slightly by day 2454. The line flux for Hα is approximately constant from day 433 to day 881. It decreases by about a factor of five by days 1766 and 2454. Other strong lines in the spectrum include [O II] λλ7319, 7330, [O III] λ4363, [O III] λλ4959, 5007, [Ne III] λ3968, He I λ5876 + Na I D (probably each of equal strength), Hβ, and [O I] λλ6300, 6364. These lines, and their relative ratios, agree fairly well with other studies of interacting SNe at late times (e.g., F99). While the circumstellar interaction model of CF94 predicts some lines that do not appear, and that [O II] λλ7319, 7330 should be weak, the model is somewhat consistent with the general line-intensity ratios, and the predicted evolution of the line ratios agrees with the observations. Our spectra, though, indicate that the density is probably higher than that used by CF94. This may be because SN 1993J is unusual, but it is inconsistent with both the power-law model that assumes a compact progenitor and the RSG model that has a more extended progenitor. Considering SN 1993J and the four SNe of F99, the power-law model appears to be a better match in its predictions, although a higher density may be required to reproduce accurately the observed line-intensity ratios.

The late-time oxygen lines imply a relatively high density ($n_e \approx 10^7$–10^8 cm^{-3}) on day 670, decreasing to $n_e \approx 10^6$–10^7 cm^{-3} by day 2454, assuming a temperature of 10,000 K. The low ratio [O III] ($\lambda\lambda$4959, 5007/λ4363) ≈ 1 at early times excludes temperatures much below 10,000 K. The increase of this ratio to ~ 3 on day 2454 shows the general expansion of the oxygen-emitting region. The appearance of the two-horned profile on the oxygen lines by day 1766 exhibits the development of emission from a somewhat flattened, disklike structure in the interaction region. This may indicate a preexisting equatorial belt of circumstellar material around SN 1993J, possibly similar to that observed in SN 1987A (e.g., Panagia et al. 1996 and references therein), although the emission in SN 1993J is likely the result of the ejecta colliding with the equatorial belt to produce the emission.

This research was supported by NSF grants AST 91-15174 and AST 94-17213 to A. V. F as well as by NASA through grants GO-7434, GO-7821 and GO-8243 from the Space Telescope Science Institute, which is operated by the Association of Universities for Research in Astronomy, Inc., under NASA contract NAS 5-26555. We are grateful to the staffs of the Lick and Keck observatories for their assistance with the observations. The W. M. Keck Observatory is operated as a scientific partnership among the California Institute of Technology, the University of California, and NASA. The observatory was made possible by the generous financial support of the W. M. Keck Foundation.

APPENDIX

TELLURIC ABSORPTION

One aspect of spectroscopy that is often overlooked in the study of SNe is the impact of weak telluric absorption, which can sometimes mimic intrinsic absorption features in SN spectra. Virtually all observers are familiar with the prominent A-band ($\sim$7600 Å) and B-band ($\sim$6850 Å) absorptions produced by molecular oxygen, and some make an attempt to remove them. There are also several strong water absorption bands in the near-IR region. Weaker water bands in the range 5000–6700 Å, however, are much less well known. Typical SN spectra are often so noisy that the weaker absorptions are not obvious. This is especially true at blue wavelengths where detectors are usually less efficient; for example, there are ozone absorption features in the region 3200–3450 Å (the Huggins bands; e.g., Schachter, Filippenko, & Kahn 1989; Schachter 1991, and references therein). An extremely weak absorption, the Chappuis ozone band, extends from 5000 Å to 7000 Å, but it is unlikely to affect SN spectra significantly (see, e.g., Kondratyev 1969). Even in spectra with a moderate S/N, some of the weaker bands can appear at high air mass or high humidity. The fortuitous appearance of a few relatively bright SNe in the past decade, however, shows that these features will be present even at low air mass in the spectra of all objects.

Figure 15 displays spectra of three bright SNe (SN 1993J, SN 1994D, and SN 1999em) over the range 6360–6700 Å. Each appears to contain an absorption line at $\sim$6515 Å, but the spectra are shown with *observed* wavelengths, and these three SNe have differing redshifts (-140 km s^{-1}, 850 km s^{-1}, and 720 km s^{-1}, respectively), clearly implying a local source for the absorption. Figure 16 is a plot of the telluric absorption spectrum as determined from solar observations obtained with the Fourier-transform spectrometer at the McMath-Pierce telescope at Kitt Peak National Observatory[5] (Wallace, Hinkle, & Livingston 1993, 1998). This telluric absorption spectrum has had the amount of water absorption increased by a factor of 1.7 to match better the conditions at Lick Observatory (G. Marcy 1999, personal communication), and it has been smoothed to correspond to a spectral dispersion of $\sim$2 Å pixel^{-1}. The inset of Figure 16 shows the telluric absorption in the region 6250–6670 Å. Note that at this resolution a strong, narrow absorption appears at 6515 Å within a broader water band.

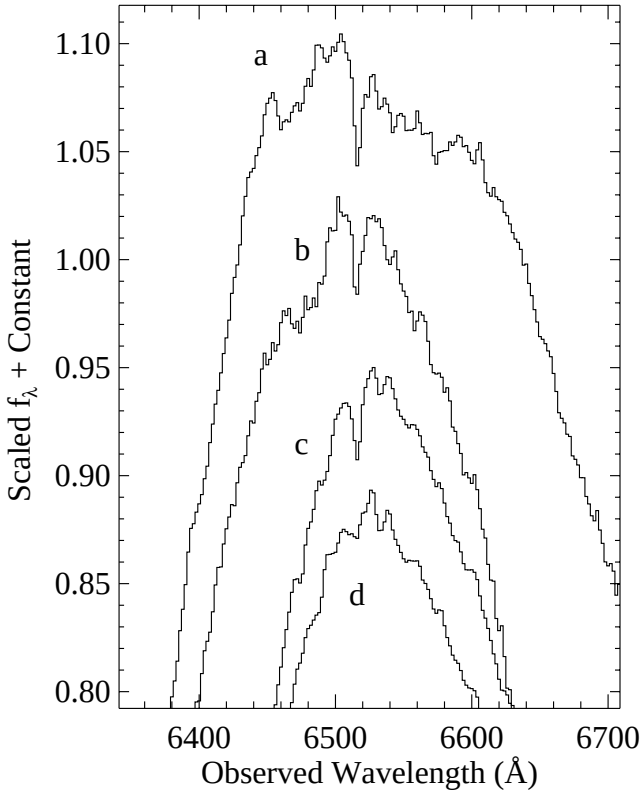

FIG. 15.—Spectra of three bright SNe illustrating the potential impact of weak telluric absorption on high S/N spectra. Spectrum (a) is SN 1993J from day 19 (1993 April 15), (b) is SN 1994D from 1994 April 18, (c) is SN 1999em from 1999 November 5, and (d) is the same SN 1999em spectrum after an attempt to remove some of the effects of telluric absorption. All three SNe were observed with the same instrument, but have different redshifts, indicating that the feature at 6515 Å is not intrinsic to the SNe. When telluric effects are considered, the feature can be removed reasonably well. Note the presence of even weaker features (such as around 6470 Å) which we did not attempt to remove.

The presence of the absorption at 6515 Å and other, weaker features near Hα indicates that great caution must be taken when interpreting small-scale fluctuations in spectra near this wavelength range. This telluric line was noted and discussed as a possibly intrinsic feature in SN 1993J by Wheeler & Filippenko (1996) and Finn et al. (1995), although neither group attributed any significance to it. Since even experienced spectroscopists can be fooled by this line, it is important to be reminded of the potential

[5] NSO/Kitt Peak FTS data used here were produced by NSF/NOAO.

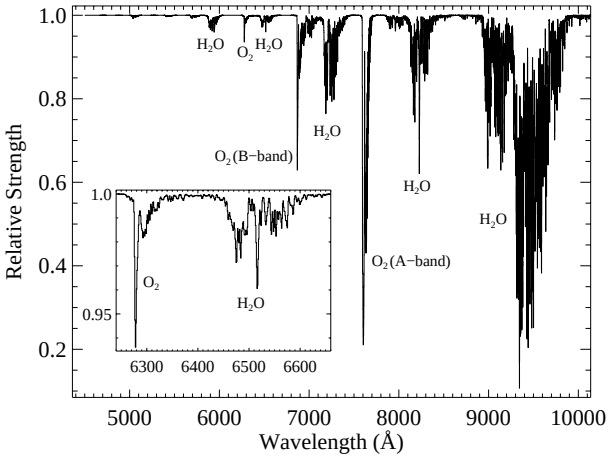

FIG. 16.—Spectrum of telluric absorption as determined from solar Fourier-transform spectra from the National Solar Observatory database at an air mass of 1.0. The spectrum has been smoothed to 2 Å pixel^{-1}, and the relative strength of the water features is enhanced (see text). The inset shows the region around the narrow feature at 6515 Å.

effects of weak telluric absorption. This is especially true in efforts to search for the presence of Hα in spectra of SNe Ia. A bright SN Ia would be an obvious choice for such an analysis, but a brighter object is more likely to show the effects of telluric absorption and lend itself to misinterpretation. The presence or absence of hydrogen in emission or absorption in the spectra of SNe Ia could have tremendous significance in the evaluation of their proposed progenitor systems (see, e.g., Branch et al. 1995). One must therefore be very careful with SN data to avoid the pitfalls of telluric absorption. With the development of ever larger telescopes, this problem will extend to even fainter SNe. In addition, the (relatively) strong O_2 absorption near 6260–6340 Å can appear to be an intrinsic SN feature in spectra with a low S/N.

It is possible to remove most of the effects of telluric absorption, especially at high spectral resolution. The division by the spectrum of a comparison star that is intrinsically featureless in the wavelength regions affected by absorption can correct object spectra fairly well (Wade & Horne 1988; Bessell 1999). It can sometimes be difficult to find a star that is sufficiently featureless at the wavelengths of interest. This technique requires a well-exposed star to minimize the addition of any noise to the object spectrum. It is preferable to have a comparison star that is observed at an air mass similar to the object, but it is possible to scale the comparison star to match. We use our own procedures to remove telluric absorption following the technique of Wade & Horne (1988).[6]

In the normal course of data reduction, we remove the stronger telluric absorptions, but we only include the regions of weaker bands when observing at high air mass (or sometimes when the humidity is high). This is to avoid adding undue noise in these regions when the weak bands are already hidden in the noise of the spectrum. High S/N objects, though, will show the weak bands. When we make an extra effort to remove them, as shown in Figure 15 for the 6515 Å line in SN 1999em, we achieve some success. There are still residuals at 6515 Å; it appears unlikely that any telluric absorption removal scheme can be 100% effective, but it can be done to a fairly good level, as long as interpretation of the spectra includes consideration of its effects. Observers must make sure that only real lines are identified as such.

[6] We note that the IRAF task TELLURIC divides the object by the comparison star properly, but does not scale the spectrum of the comparison star according to the method of Wade & Horne (1988). With both TELLURIC and Wade & Horne, the comparison star is exponentiated by a function of the ratio of the air masses of the object and the comparison star. In TELLURIC, however, this function is the ratio of air masses multiplied by a scale factor, while with Wade & Horne it is the ratio of the air masses raised to a power. Wade & Horne choose a power as the strongest telluric lines are saturated and the equivalent widths will grow with approximately the square root of the air mass. The TELLURIC scaling of the ratio of the air masses effectively assumes an optically thin atmospheric absorption. When the air masses of object and comparison star are similar, this different treatment has little impact. With the Wade & Horne method, variation of the power depending on the source and level of saturation of the absorption may result in better removal. We are conducting tests in this area.

REFERENCES

Aldering, G., Humphreys, R. M., & Richmond, M. 1994, AJ, 107, 662
Almog, Y., & Netzer, H. 1989, MNRAS, 238, 57
Anderson, M. C., Jones, T. W., Rudnick, L., Tregillis, I. L., & Kang, H. 1994, ApJ, 421, L31
Andronova, A. A. 1992, Soviet Astron. Lett., 18, 360
Aretxaga, I., Benetti, S., Terlevich, R. J., Fabian, A. C., Cappellaro, E., Turatto, M., & Della Valle, M. 1999, MNRAS, 309, 343
Aschenbach, B., Egger, R., & Trümper, J. 1995, Nature, 373, 587
Baade, W., & Minkowski, R. 1954, ApJ, 119, 206
Barbon, R., Benetti, S., Cappellaro, E., Patat, F., Turatto, M., & Iijima, T. 1995, A&AS, 110, 513
Benetti, S., Cappellaro, E., Danziger, I. J., Turatto, M., Patat, F., & Della Valle, M. 1998, MNRAS, 294, 448
Bessell, M. S. 1999, PASP, 111, 1426
Blondin, J. M., Lundqvist, P., & Chevalier, R. A. 1996, ApJ, 472, 257
Bouchet, P., Lawrence, S., Crotts, A., Sugerman, B., Uglesich, R., & Heathcote, S. 2000, IAU Circ. 7354
Branch, D., Livio, M., Yungelson, L. R., Boffi, F. R., & Baron, E. 1995, PASP, 107, 1019
Cappellaro, E., Danziger, I. J., & Turatto, M. 1995, MNRAS, 277, 106
Cardelli, J. A., Clayton, G. C., & Mathis, J. S. 1989, ApJ, 345, 245
Chevalier, R. A., & Blondin, J. M. 1995, ApJ, 444, 312
Chevalier, R. A., Blondin, J. M., & Emmering, R. T. 1992, ApJ, 392, 118
Chevalier, R. A., & Fransson, C. 1989, ApJ, 343, 323
———. 1992, ApJ, 395, 540
———. 1994, ApJ, 420, 268 (CF94)
Chu, Y.-H., Caulet, A., Montes, M., Panagia, N., Van Dyk, S. D., & Weiler, K. W. 1999, ApJ, 512, L51
Chugai, N. N. 1992, Soviet Astron. Lett., 18, 239
———. 1994, ApJ, 428, L17
———. 1986, Sov. Astron., 30, 563
Chugai, N. N., Danziger, I. J., & Della Valle, M. 1995, MNRAS, 276, 530
Clocchiatti, A., Wheeler, J. C., Barker, E. S., Filippenko, A. V., Matheson, T., & Liebert, J. W. 1995, ApJ, 446, 167
Fassia, A., Meikle, W. P. S., Geballe, T. R., Walton, N. A., Pollacco, D. L., Rutten, R. G. M., & Tinney, C. 1998, MNRAS, 299, 150
Fesen, R. A. 1993, ApJ, 413, L109
———. 1998, AJ, 115, 1107
Fesen, R. A., & Becker, R. H. 1990, ApJ, 351, 437
Fesen, R. A., et al. 1999, AJ, 117, 725 (F99)
Fesen, R. A., & Matonick, D. M. 1993, ApJ, 407, 110
———. 1994, ApJ, 428, 157
Filippenko, A. V. 1989, AJ, 97, 726
———. 1991a, in Supernovae, ed. S. E. Woosley (New York: Springer), 467
———. 1991b, in SN 1987A and Other Supernovae, eds. I. J. Danziger & K. Kjär (Garching: ESO), 343
Filippenko, A. V., Matheson, T., & Barth, A. J. 1994, AJ, 108, 2220 (FMB94)
Filippenko, A. V., Matheson, T., & Ho, L. C. 1993, ApJ, 415, L103 (FMH93)
Filippenko, A. V., & Sargent, W. L. W. 1989, ApJ, 345, L43

Finn, R. A., Fesen, R. A., Darling, G. W., Thorstensen, J. R., & Worthey, G. S. 1995, AJ, 110, 300
Fransson, C. 1984, A&A, 133, 264
Fransson, C., Lundqvist, P., & Chevalier, R. A. 1996, ApJ, 461, 993
Freedman, W. L., et al. 1994, ApJ, 427, 628
Gerardy, C. L., Fesen, R. A., Höflich, P., & Wheeler, J. C. 2000, AJ, 119, 2968
Haas, M. R., Colgan, S. W. J., Erickson, E. F., Lord, S. D., Burton, M. G., & Hollenbach, D. J. 1990, ApJ, 360, 257
Hachisu, I., Matsuda, T., Nomoto, K., & Shigeyama, T. 1991, ApJ, 368, L27
Hanuschik, R. W., Spyromilio, J., Stathakis, R., Kimeswenger, S., Gochermann, J., Seidensticker, K. J., & Meurer, G. 1993, MNRAS, 261, 909
Houck, J. C., & Fransson, C. 1996, ApJ, 456, 811
Iwamoto, K., Young, T. R., Nakasato, N., Shigeyama, T., Nomoto, K., Hachisu, I., & Saio, H. 1997, ApJ, 477, 865
Kingdon, J., Ferland, G. J., & Feibelman, W. A. 1995, ApJ, 439, 793
Khokhlov, A. M., Höflich, P. A., Oran, E. S., Wheeler, J. C., Wang, L., & Chtchelkanova, A. Yu. 1999, ApJ, 524, L107
Kifonidis, K., Plewa, T., Janka, H.-Th., & Müller, E. 2000, ApJ, 531, L123
Kondratyev, K. Ya. 1969, Radiation in the Atmosphere (New York: Academic Press)
Leibundgut, B., Kirshner, R. P., Pinto, P. A., Rupen, M. P., Smith, R. C., Gunn, J. E., & Schneider, D. P. 1991, ApJ, 372, 531
Leonard, D. C., Filippenko, A. V., Barth, A. J., & Matheson, T. 2000, ApJ, 536, 239
Lewis, J. R., et al. 1994, MNRAS, 266, L27
Li, A., Hu, J., Wang, L., Jiang, X., & Li, H. 1994, Ap&SS, 211, 323
Li, H., & McCray, R. 1992, ApJ, 387, 309
———. 1993, ApJ, 405, 730
Livne, E., Tuchman, Y., & Wheeler, J. C. 1992, ApJ, 399, 665
Long, K. S., Blair, W. P., & Krzeminski, W. 1989, ApJ, 340, L25
Marcaide, J. M., et al. 1997, ApJ, 486, L31
Marietta, E., Burrows, A., & Fryxell, B. 2000, ApJ, submitted (astro-ph/9908116)
Matheson, T., et al. 2000, AJ, 120, 1487 (Paper I)
Nomoto, K., Suzuki, T., Shigeyama, T., Kumagai, S., Yamaoka, H., & Saio, H. 1993, Nature, 364, 507
O'Donnell, J. E. 1994, ApJ, 422, 158
Panagia, N., Scuderi, S., Gilmozzi, R., Challis, P. M., Garnavich, P. M., & Kirshner, R. P. 1996, ApJ, 459, L17
Patat, F., Chugai, H., & Mazzali, P. A. 1995, A&A, 299, 715
Richmond, M. W., Treffers, R. R., Filippenko, A. V., & Paik, Y. 1996, AJ, 112, 732
Richmond, M. W., Treffers, R. R., Filippenko, A. V., Paik, Y., Leibundgut, B., Schulman, E., & Cox, C. V. 1994, AJ, 107, 1022
Ryder, S., Staveley-Smith, L., Dopita, M., Petre, R., Colbert, E., Malin, D., & Schlegel, E. 1993, ApJ, 416, 167
Schachter, J. 1991, PASP, 103, 457
Schachter, J., Filippenko, A. V., & Kahn, S. M. 1989, ApJ, 340, 1049
Schlegel, D. J., Finkbeiner, D. P., & Davis, M. 1998, ApJ, 500, 525
Schlegel, E. M. 1990, MNRAS, 244, 269
Schlegel, E. M., & Kirshner, R. P. 1989, AJ, 98, 577
Shigeyama, T., Nomoto, K., Tsujimoto, T., & Hashimoto, M. 1990, ApJ, 361, L23
Spyromilio, J. 1991, MNRAS, 253, 25P
———. 1994, MNRAS, 266, L61 (S94)
Spyromilio, J., Meikle, W. P. S., & Allen, D. A. 1990, MNRAS, 242, 669
Spyromilio, J., & Pinto, P. A. 1991, in SN 1987A and Other Supernovae, eds. I. J. Danziger & K. Kjär (Garching: ESO), 423
Spyromilio, J., Stathakis, R. A., & Meurer, G. R. 1993, MNRAS, 263, 530
Stathakis, R. A., Dopita, M. A., Cannon, R. D., & Sadler, E. M. 1991, in Supernovae, ed. S. E. Woosley (New York: Springer), 95
Stathakis, R. A., & Sadler, E. M. 1991, MNRAS, 250, 786
Strom, R., Johnston, H. M., Verbunt, F., & Aschenbach, B. 1995, Nature, 373, 590
Swartz, D. A. 1991, in Supernovae, ed. S. E. Woosley (New York: Springer), 434
Swartz, D. A., Clocchiatti, A., Benjamin, R., Lester, D. F., & Wheeler, J. C. 1993, Nature, 365, 232
Swartz, D. A., Harkness, R. P., & Wheeler, J. C. 1989, Nature, 337, 439
Trammell, S. R., Hines, D. C., & Wheeler, J. C. 1993, ApJ, 414, L21
Tran, H. D., Filippenko, A. V., Schmidt, G. D., Bjorkman, K. S., Jannuzi, B. T., & Smith, P. S. 1997, PASP, 109, 489
Turatto, M., Cappellaro, E., Danziger, I. J., Benetti, S., Gouiffes, C., & Della Valle, M. 1993, MNRAS, 262, 128
Uomoto, A. 1991, AJ, 101, 1275
Utrobin, V. 1994, A&A, 281, L89
Van Dyk, S. D., Weiler, K. W., Sramek, R. A., Rupen, M. P., & Panagia, N. 1994, ApJ, 324, L115
Wade, R. A., & Horne, K. D. 1988, ApJ, 324, 411
Wallace, L., Hinkle, K., & Livingston, W. 1993, An Atlas of the Photospheric Spectrum from 8900 to 13,600 cm^{-1} (7350 to 11,230 Å) (NSO: Tech. Rep. 93-001) (Tucson: NSO)
———. 1998, An Atlas of the Spectrum of the Solar Photosphere from 13,500 to 28,000 cm^{-1} (3570 to 7405 Å) (NSO: Tech. Rep. 98-001) (Tucson: NSO)
Wang, L., Howell, D. A., Höflich, P., & Wheeler, J. C. 2000, ApJ, submitted (astro-ph/9912033)
Wang, L., & Hu, J. 1994, Nature, 369, 380
Wheeler, J. C., et al. 1993, ApJ, 417, L71
Wheeler, J. C., & Filippenko, A. V. 1996, in Supernovae and Supernova Remnants, ed. R. A. McCray & Z. Wang (Cambridge: Cambridge Univ. Press), 241
Wheeler, J. C., Harkness, R. P., Barker, E. S., Cochran, A. L., & Wills, D. 1987, ApJ, 313, L69
Wheeler, J. C., Swartz, D. A., & Harkness, R. P. 1993, Phys. Rep., 227, 113
Winkler, P. F., & Kirshner, R. P. 1985, ApJ, 299, 981
Woosley, S. E., Eastman, R. G., Weaver, T. A., & Pinto, P. A. 1994, ApJ, 429, 300
Woosley, S. E., Langer, N., & Weaver, T. A. 1995, ApJ, 448, 315